UNIVERSIDADE ESTADUAL DE CAMPINAS
FACULDADE DE ENGENHARIA ELÉTRICA E DE COMPUTAÇÂO

Benjamin Sarti

Field Calibration Procedure for Enhanced Automatic Gain Control of Distributed Counter-Propagating Raman Amplifiers

Processo de Calibração em Campo de Amplificadores Raman Distribuídos Contra-Propagantes para Aprimoramento do Controle Automático de Ganho

CAMPINAS
2015

Benjamin Sarti

Field Calibration Procedure for Enhanced Automatic Gain Control of Distributed Counter-Propagating Raman Amplifiers

Processo de Calibração em Campo de Amplificadores Raman Distribuídos Contra-Propagantes para Aprimoramento do Controle Automático de Ganho

Masters dissertation presented at the School of Electrical and Computer Engineering of the University of Campinas in partial fulfillment of the requirements for the degree of Master in Electrical Engineering. Concentration area: Telecommunications and Telematics.

Dissertação de Mestrado apresentada na Faculdade de Engenharia Elétrica e de Computação da Universidade Estadual de Campinas como parte dos requisitos exigidos para a obtenção do título de Mestre em Engenharia Elétrica. Área de concentração: telecommunicações e telemática.

Supervisor: Prof. Dr. Max Henrique Machado Costa

Este exemplar corresponde à versão final da dissertação de Mestrado defendida pelo aluno Benjamin Sarti, e orientada pelo Prof. Dr. Max Henrique Machado Costa.

CAMPINAS
2015

Agência(s) de fomento e nº(s) de processo(s): Não se aplica.

Ficha catalográfica
Universidade Estadual de Campinas
Biblioteca da Área de Engenharia e Arquitetura
Luciana Pietrosanto Milla - CRB 8/8129

Sa77f

Sarti, Benjamin, 1990-
Field calibration procedure for enhanced automatic gain control of distributed counter-propagating Raman amplifiers / Benjamin Sarti. – Campinas, SP : [s.n.], 2015.

Orientador: Max Henrique Machado Costa.
Dissertação (mestrado) – Universidade Estadual de Campinas, Faculdade de Engenharia Elétrica e de Computação.

1. Amplificadores distribuídos. 2. Raman, Efeito de. 3. Controle automático. 4. Calibração. I. Costa, Max Henrique Machado,1950-. II. Universidade Estadual de Campinas. Faculdade de Engenharia Elétrica e de Computação. III. Título.

Informações para Biblioteca Digital

Título em outro idioma: Processo de calibração em campo de amplificadores Raman distribuídos contra-propagantes para aprimoramento do controle automático de ganho
Palavras-chave em inglês:
Distributed amplifiers
Raman, Effect
Automatic control
Calibration
Área de concentração: Telecomunicações e Telemática
Titulação: Mestre em Engenharia Elétrica
Banca examinadora:
Max Henrique Machado Costa [Orientador]
Marcelo Eduardo Vieira Segatto
Aldário Chrestani Bordonalli
Data de defesa: 10-12-2015
Programa de Pós-Graduação: Engenharia Elétrica

JUDGING COMMITTEE - MASTERS DISSERTATION
(COMISSÃO JULGADORA - DISSERTAÇÃO DE MESTRADO)

Candidate (Candidato): Benjamin Sarti
Defense date (Data da defesa): December 10th, 2015 (10 de Dezembro de 2015)

Thesis Title: "Field Calibration Procedure for Enhanced Automatic Gain Control of Distributed Counter-Propagating Raman Amplifiers."
Título da Tese: "Processo de Calibração em Campo de Amplificadores Raman Distribuídos Contra-Propagantes para Aprimoramento do Controle Automático de Ganho."

Prof. Dr. Max Henrique Machado Costa (President, FEEC/UNICAMP)
Prof. Dr. Eduardo Vieira Segatto (UFES)
Prof. Dr. Aldário Chrestani Bordonalli (FEEC/UNICAMP)

The attestation of defense, with the respective signatures of the Judging Committee, can be found in the student's academic life file.
A ata de defesa, com as respectivas assinaturas dos membros da Comissão Julgadora, encontra-se no processo de vida acadêmica do aluno.

Acknowledgement

First of all, I would like to thank Prof. Dr. Max Henrique Machado Costa for his guidance, incentive and friendship.

Thanks to CPqD Foundation for encouraging me in this project, for releasing many hours of work to study subjects of my interest at the University of Campinas and for funding this research. A special thanks to Uiara Celine de Moura and Dr. Juliano Rodrigues Fernandes de Oliveira that gave me a huge optical amplifiers background for this work. Thanks also to Dr. Miquel Garrich Alabarce for following my activities at CPqD and to Israel Jacob Galego Casimiro and Benoît François Marie Christian Roulle for implementing the field calibration procedure in the amplifier's firmware for the experimental validation.

Thanks to my parents Brigitte and Jean-Claude, my sister Julie, her fiance Thibaut and my niece Emy for sending me good vibes from France.

Thanks to my friend Israel for being there for me every time I need a support. Thank you also for teaching me Portuguese and for being so honest.

Thanks to my friends Aline, Juju and Camila for training with me at the weight room every night. You make my training really entertaining.

Thanks to my childhood friend Vincent for playing tennis with me and for sharing so many experiences.

Thanks to my Chilean friends Rodolfo, Alfonso and Camilo, my Mexican friends Juan and Pepe and my Brazilian friend Victor that I knew at École Centrale Marseille and that studied, played, watched animations and traveled with me. Thank you also for making me want to discover your beautiful continent.

Thanks to my high school friends Bérangère, Morgane, Mohamed and Julien that keep in touch with me and that I see every time I go back to France.

Field Calibration Procedure for Enhanced Automatic Gain Control of Distributed Counter-Propagating Raman Amplifiers

Abstract

Distributed Raman amplifiers (DRAs) have gained interest for elastic optical networking (EON) because they allow, in some configurations, to increase the amplification bandwidth, to enhance the gain flatness and to decrease the noise insertion compared to conventional erbium doped fiber amplifiers (EDFAs). However, there are operational issues in the deployment of DRAs because the transmission fiber itself serves as the gain medium. The characteristics of this fiber, that are not always perfectly known in field installations, have an influence on the Raman gain used for the signal amplification. As a consequence, the pump power of the DRAs must be adjusted to adapt to the actual fiber properties to provide accurate automatic gain control.

This Masters dissertation presents a field calibration procedure for distributed counter-propagating Raman amplifiers to enhance their automatic gain control. The performance of this calibration procedure is demonstrated in simulations for transmission fibers of different attenuation profiles and is validated experimentally with fibers of different attenuation profiles and with splices located at several distances from the DRA pump lasers. Finally, the impact of this calibration procedure on the amplifiers gain flatness and noise figure is presented in simulations.

Keywords: Distributed counter-propagating Raman amplifiers, Automatic Gain Control, Field Calibration.

Processo de Calibração em Campo de Amplificadores Raman Distribuídos Contra-Propagantes para Aprimoramento do Controle Automático de Ganho

Resumo

Os amplificadores Raman distribuídos (DRAs) têm se mostrado interessantes nas redes ópticas elásticas porque eles permitem, em algumas configurações, aumentar a banda de amplificação, melhorar a planicidade dos canais e diminuir a inserção de ruído em relação aos amplificadores a fibra dopada com érbio (EDFAs) convencionais. No entanto, existem problemas operacionais nos DRAs pois a amplificação acontece na própia fibra de transmissão. As características desta fibra, que não são sempre perfeitamente conhecidas nas instalações em campo, têm uma influência sobre o ganho Raman utilizado para a amplificação do sinal. Como consequência, os lasers de bombeio dos DRAs devem ser ajustados para se adaptar as propriedades da fibra de maneira a providenciar um controle automático de ganho preciso.

Esta dissertação de Mestrado apresenta um processo de calibração em campo dos amplificadores Raman distribuídos contra-propagantes para melhorar a precisão do controle automático de ganho. A eficiência deste processo é demonstrada em simulação para fibras de transmissão tendo diferentes perfis de atenuação e é validada experimentalmente com fibras tendo diferentes perfis de atenuação e com emendas localizadas a várias distâncias dos lasers de bombeio dos DRAs. Enfim, o impacto do processo de calibração na planicidade do ganho e na figura de ruído do amplificador é apresentado em simulação.

Palavras-chave: Amplificadores Raman Distribuídos Contra-Propagantes, Controle Automático de Ganho, Calibração em Campo.

Procédure de Calibration sur le Terrain des Amplificateurs Raman Distribués Contre-Propagatifs pour Améliorer la Précision de leur Controle Automatique de Gain

Résumé

L'utilisation d'amplificateurs Raman distribués (DRAs) devient de plus en plus intéressante dans les réseaux optiques élastiques car ils permettent, dans certaines configurations, d'augmenter la bande d'amplification, de rendre la courbe de gain plus plate et de diminuer l'insertion de bruit par rapport aux amplificateurs à fibre dopée à l'erbium (EDFAs) conventionnels. Pour autant, il y a des problèmes opérationnels avec les DRAs puisque l'amplification a lieu dans la fibre de transmission. Les caractéristiques de cette fibre, qui ne sont pas parfaitement connues dans les installations sur le terrain, ont une influence directe sur le gain Raman utilisé pour l'amplification du signal. Par conséquent, les lasers de pompe des DRAs doivent être ajustés pour s'adapter aux propriétés de la fibre de manière a garantir un controle automatique de gain précis.

Cette dissertation de Master présente une procédure de calibration sur le terrain des amplificateurs Raman contre-propagatifs distribués pour améliorer la precision de leur controle automatique de gain. L'efficacité de cette procédure est démontrée en simulation pour des fibres de transmission ayant différents profils d'attenuations et est validée experimentallement avec des fibres ayant différents profils d'attenuations et avec des épissures situées à plusieurs distances des lasers de pompe des DRAs. Enfin, l'impact de la procédure de calibration sur la courbe de gain et sur le facteur de bruit de l'amplificateur est présenté dans des résultats en simulation.

Mots clés: Amplificateurs Raman Distribués Contre-Propagatifs, Controle Automatique de Gain, Calibration sur le Terrain.

List of Figures

List of Abbreviations

AC	After calibration
AGC	Automatic gain control
ASE	Amplified spontaneous emission
BC	Before calibration
BVT	Bandwidth-variable transponder
DCF	Dispersion compensating fiber
DRA	Distributed Raman amplifier
DSF	Dispersion shifted fiber
DWDM	Dense davelength-division multiplexing
EDF	Erbium doped fiber
EDFA	Erbium doped fiber amplifier
EON	Elastic optical network
GCP	Gain control polynomial
GFF	Gain flattening filter
LRA	Lumped Raman amplifier
NF	Noise figure
OEO	Optical-electrical-optical
OSNR	Optical signal-to-noise ratio
OTDR	Optical time-domain reflectometer
PC	Pump combiner
PD	Photodetector
PI	Proportional-integral
ROADM	Reconfigurable optical add-drop multiplexer
SMF	Single-mode fiber
SNR	Signal-to-noise ratio
SRS	Stimulated Raman scattering
SSMF	Standard single-mode fiber
WDM	Wavelength-division multiplexing

List of Symbols

DR	Dynamic range (in dB)
F	Fiber profile
G	Gain (in dB)
G_{on-off}	On-off gain (in dB)
$Loss$	Fiber loss (in dB)
Max	Maximum AGC error (in dB)
$Mean$	Average of the AGC errors (in dB)
Min	Minimum AGC error (in dB)
NF	Noise figure (in dB)
P_{in}	Total input power of the amplifier (in dBm)
P_{in}^{MAX}	Maximum total input power of the amplifier (in dBm)
P_{in}^{MIN}	Minimum total input power of the amplifier (in dBm)
P_{launch}	Launch power into the optical fiber (in dBm)
P_{nom}	Nominal power of the laser (in mW)
P_{off}	Total output power of the amplifier with the lasers turned off (in dBm)
P_{off}^{MAX}	Maximum total output power of the amplifier with the lasers turned off (in dBm)
P_{off}^{MIN}	Minimum total output power of the amplifier with the lasers turned off (in dBm)
P_{on}	Total output power of the amplifier with the lasers turned on (in dBm)
P_{on}^{MAX}	Maximum total output power of the amplifier with the lasers turned on (in dBm)
P_{on}^{MIN}	Minimum total output power of the amplifier with the lasers turned on (in dBm)
P_{out}	Total output power of the amplifier (in dBm)
P_{out}^{MAX}	Maximum total output power of the amplifier (in dBm)
P_{out}^{MIN}	Minimum total output power of the amplifier (in dBm)
ΔP_{pump}^{GR+1}	Pump power variation necessary to increase the real gain of 1 dB (in mW)
P_{pump}	Laser pump power (in mW)
$ripple$	Ripple of the optical signal (in dB)
RG	Real gain (in dB)
RP_{out}	Real output power of the amplifier (in dBm)
TG	Target gain (in dB)
TG_X	Target gain of X dB
TP_{out}	Target output power of the amplifier (in dBm)

Contents

Chapter 1

Introduction

With the dramatic growth of Internet-based services, such as file sharing, social networking, cloud computing and Internet video, current optical networks must support an increase of traffic demand to ensure high-speed connectivity to end-users [1]. To meet these requirements, advanced modulation formats are investigated and implemented to enhance network performance in terms of capacity, quality and high spectral efficiency. In particular, current research trends on elastic optical networking (EON) are proposing node architectures that route arbitrary channel bandwidths and bandwidth-variable transponders (BVTs) [2]. The use of these advanced modulation formats in EONs requires high optical signal-to-noise ratio (OSNR) to guarantee error free reception. In this context, optical amplification plays a crucial role since it recovers optical signals from attenuations due to fibers and reconfigurable optical add-drop multiplexers (ROADMs) but it also inserts noise in wavelength division multiplexing (WDM) systems. Therefore, optical amplifiers must be designed to deliver acceptable gains in the optical bandwidth and to limit noise insertion. Two main technologies of optical amplifiers are deployed in current WDM systems.

On the one hand, the erbium doped fiber amplifier (EDFA) is a concentrated amplifier, which means that it amplifies the optical signal in specific points of the fiber link, using several meters of erbium doped fiber. It became popular before the 2000s because of its high pumping efficiency to amplify low power signals. Therefore, high gains can be achieved (>40 dB) using few meters of erbium doped fiber. Moreover, simple automatic gain control (AGC) closed-loop schemes can be implemented. Indeed, the input and the output powers of concentrated amplifiers can be measured and the target gain can be obtained by acting on the pump power. However, the EDFA provides amplification over a limited spectrum width (35 nm), which is a limitation in current optical networks that require always more optical bandwidth [3].

On the other hand, the Raman amplifier can be developed using two topolo-

gies. The lumped Raman amplifier is, like in the EDFA case, a concentrated amplifier. It amplifies the signal using about one kilometer of dispersion compensating fiber. The other topology is the distributed Raman amplifier (DRA) where the amplification occurs along several kilometers of transmission fiber. Both topologies, lumped and distributed, present low pumping efficiency for the amplification, which prevented their utilization in WDM systems for a long time. Nowadays, powerful lasers have become cheaper due to large scale production and Raman amplifiers have regained interest. Furthermore, by properly choosing the number of pumps and their wavelengths, Raman amplifiers enable flat gains and a large amplification bandwidth (>100 nm) [4]. In terms of noise insertion, the DRA has an advantage over the EDFA and the lumped Raman because its distributed signal amplification along the transmission fiber allows lower noise figures [5]. Thus, the DRA becomes suitable for long-haul (from 300 km to 800 km) and ultra-long-haul (above 800 km) systems that use advanced modulation formats. The main drawback arises when controlling the amplifier using the previously refered AGC mode. When using AGC for the DRA, the pump power is usually set blindly since, in general, there is no access to the input power, which is the launch power into the fiber span. Therefore, the amplifier actual gain cannot be measured and the AGC accuracy cannot be guaranteed. In this context, our work, that focus on distributed counter-propagating Raman amplifiers, is motivated by the following observation.

Several laboratorial procedures allow to adjust the pump power of the DRA to provide the desired gain. However, the gain of the amplifier depends on the characteristics of the transmission fiber [6]. Consequently, these laboratory pump power adjustments are not valid any more with a fiber that does not have the same characteristics as the laboratorial one. In field installations, the fiber may suffer aging, bending, addition of splices or connectors which change its properties. Therefore, these laboratory pump power adjustments are not reliable for accurate automatic gain control.

Many works in the literature already present solutions for controlling the DRA gain. In the patent applications US 20120177366 A1 (Method and arrangement for in service Raman gain measurement and monitoring) [7] and US 20110141552 A1 (Automatic measurement and gain control of distributed Raman amplifiers) [8] the information given by a monitoring channel sent along with the signal at the transmission is used for gain control. Therefore, these solutions can be implemented only if a monitoring channel is available.

The patents US 8854726 B2 (Method for controlling signal gain of a Raman amplifier) [9] and US 6519082 B2 (Apparatus and method for a self-adjusting Raman amplifier) [10] aim to calculate the real-time gain of the DRA by estimating some characteristics of the in-field fiber. These characteristics are obtained by measuring with

an optical time-domain reflectometer (OTDR) the backscattered light of the signal, the pump power or a monitoring channel in the fiber. To be implemented, this technique requires additional components like optical splitters, photodetectors, components necessary for the integration of a monitoring channel and finally an OTDR. As a result, the fabrication cost is much higher.

The patent application US 20070115537 A1 (Method and an optical amplifier assembly for adjusting Raman gain) [11] presents a calibration procedure based on the analysis of the power transient after removing or adding channels at the transmission side. This procedure is only efficient if the target gain remains the same, which is a limitation.

The patent application US 20120327505 A1 (Method of performing target Raman gain locking and Raman fiber amplifier) [12] describes a gain control based on the measurement of the amplified spontaneous emission (ASE) out of the optical channels band. To do so, a calibration procedure is needed. This calibration consists in establishing a linear relation between the Raman gain and the ASE noise produced in the amplification process. To implement this solution, additional components are necessary for the ASE measurement like an optical filter and a photodetector.

The patent application EP 1508985 A1 (Gain monitor in a distributed Raman amplifier) [13] presents a gain control that use the modulation of the pump power by a low frequency signal. This modulation is transferred to the Raman gain. The power variations measured by the photodetectors at the output of the amplifier allow to deduce the current gain of the amplifier thanks to a linear variation. This gain control method use a modulator that increase the production cost.

The patent application US 20150002922 A1 (Self-automatic gain control distributed Raman fiber amplifier and automatic gain control method) [14] describes a method to control the gain and the gain flatness of the counter-propagating DRA with an unknown in-field fiber. In this method, the pump power efficiency of the for the amplification is evaluated. After this step, the in-field fiber is assimilated to a predetermined fiber, chosen in a database of fibers, whose characteristics are the closest to the real in-field fiber in terms of Raman amplification efficiency. By doing so, the gain control is processed by setting the pump power corresponding to the predetermined fiber that was selected. Obviously, one of the drawbacks of this solution is that this predetermined database requires memory space in the control unit. Another drawback is that this assimilation to a predetermined fiber is an approximation that can lead to gain control errors.

The patent application BR 10 2012 021156-4 (Método de controle de ganho e dispositivo amplificador óptico híbrido para redes DWDM reconfiguráveis) (in por-

tuguese) [15] presents a gain control where, for each target gain, a fifth order gain control polynomial (GCP) returns the pump power that must be set with the information of the output power of the amplifier with the lasers turned off. At the field installation of the amplifier, these GCPs are not actualized and gain control errors can occur since the in-field transmission fiber doesn't have the same characteristics as the fiber that was used to generate the GCPs.

This Master's dissertation presents a new calibration procedure that allows to control the counter-propagating DRA with accuracy in AGC mode. This calibration procedure does not require any information about the in-field fiber characteristics or about the launched signal power. Furthermore, the proposed calibration procedure can be implemented only with the traditional components that compose the DRA (pump lasers, optical couplers and splitters, photodetector and control unit) so there is no increase in the production cost.

1.1 Proposed work

1.1.1 Objectives

This work proposes an in-field calibration procedure of distributed counter-propagating Raman amplifiers for enhanced automatic gain control. This calibration procedure aims to correct the laboratorial pump power adjustments to adapt to the in-field transmission fiber. When processed, the calibration procedure evaluates the pump power efficiency for Raman amplification and thus on the Raman gain and adapt, for each operation point of the amplifier, the pump power for AGC accuracy.

1.1.2 Contributions

The principal contributions of this work are the following:

- Generation and study of the behavior of GCPs (based on the patent application BR 10 2012 021156-4 [15]) for adjustment of the pump power of the DRA for AGC;
- Proposal of a calibration procedure in field installations where these GCPs are adjusted to adapt to the real transmission fiber properties to ensure AGC accuracy at each operation point of the DRA;
- Evaluation of the proposed field calibration procedure performance in simulations considering transmission fibers of different attenuation profiles;

- Evaluation of the proposed field calibration procedure impact on the gain flatness and noise figure of the DRA in simulations;
- Experimental validation of the proposed field calibration procedure with fibers of different attenuation profiles and with splices located at several distances from the DRA pump lasers. The attenuation of theses splices is varied from 0.9 to 3.2 dB to test the calibration procedure efficiency in extreme conditions.

1.2 Chapters description

Chapter 2 presents the theoretical fundamentals necessary for the realization of this work. It includes the evolution of optical networks and a description of the main optical amplifiers technologies. The difference between these amplifier technologies is detailed and the amplifier power masks, that indicate their operational performance, are defined.

Chapter 3 details the differences of automatic gain control between concentrated and distributed amplifiers. Then, the AGC of distributed counter-propagating Raman amplifiers implemented for this work is presented.

Chapter 4 describes operational issues with the DRA when operating in the AGC mode in field installations. To overcome these operational issues, an in-field calibration procedure of the DRA for accurate AGC is proposed. To justify the proposal of this calibration procedure, a previous study of the DRA amplification behavior is performed.

Chapter 5 evaluates the proposed field calibration procedure performance in simulations considering transmission fibers of different attenuation profiles. Also, the impact of the calibration procedure on the gain flatness and noise figure of the DRA is reported.

Chapter 6 validates the proposed field calibration procedure in several experiments. The calibration procedure efficiency is evaluated for several transmission fibers presenting different attenuation profiles and having splices situated at various distances from the pump lasers.

Finally, Chapter 7 concludes this Masters dissertation.

Chapter 2

Theoretical fundamentals

Nowadays, optical networks must support an unstoppable increase of traffic demand driven by new bandwidth-hungry services and applications to ensure high speed connectivity to end-users.

In optical networks, optical amplifiers are key elements since they recover optical signals from attenuations due to fibers and ROADMs. Consequently, optical amplifiers enable long haul spans and are convenient in WDM networks since they operate in a wide optical bandwidth and can amplify various channels simultaneously.

This chapter illustrates the evolution of optical networks from the first optical transmission systems to the arrival of WDM and optical amplifiers. Then, the main optical amplifiers technologies are described and compared. Finally, the figures of merit and the power masks that indicate the operational performance of optical amplifiers are defined.

2.1 The evolution of optical networks

Optical transmission systems were demonstrated commercially for the first time in 1980 at a line rate of 45 Mb/s. They were made up of a cascade of optical links composed of a transmitter, a fiber line, and a receiver. Each optical link was followed by an OEO (optical-electrical-optical) regenerator to overcome transmission losses and regenerate the signal to reduce signal distortion in the fiber [16].

By the early 1990s, optical transmission systems could operate at ∼2 Gb/s. Most traffic was voice but fax and some data services were beginning to drive more traffic on the network.

As researchers explored optical transmission at higher bit rates (∼10 Gb/s), signal impairments on the fiber due to fiber dispersion, both chromatic and polarization, began to present issues. That was especially the case at a wavelength of 1550 nm, the

lowest loss wavelength region for silica fiber, to make up for the larger signal level need for detection at the higher rate, but where standard single mode (SSMF) fiber has nonzero dispersion [17].

Moreover, the emergence of high transmission capacity placed a tremendous burden on the electronic devices. Considering the traffic growth and possible migration of optical transmission systems to ultra-high bit rates made the electronic bottleneck a serious problem. Due to these concerns, keeping the single wavelength architecture for optical transport networks did not appear very effective.

The technical community was certainly aware of WDM as another way to increase the fiber capacity. Under WDM, the optical spectrum available in the fiber is carved up into a number of non-overlapping wavelength bands, with each wavelength supporting a single communication channel. In this way, WDM avoided the problematic transmission impairments incurred by higher bit rates as well as escaping the need to drive to higher speed electronics.

The main obstacle for commercial viability of WDM transmission systems prior to the availability of the optical amplifier was the cost of electrical regenerators. In primary WDM systems, optical propagation loss compensation was still achieved by electrical regeneration. Each wavelength in the WDM system would have to be demultiplexed and regenerated electrically, the operation so called OEO regeneration. The regenerators were required at each regeneration site to restore optical signals. In this sense, the implementation cost to upgrade the transmission system would increase roughly proportionately to the capacity increase. That was not acceptable in the marketplace [18].

At the very heart of the motivation, justification, and evolution of the WDM transmission systems and ultimately WDM optical transport networks is the enormous value proposition of the optical amplifiers. The fact that a single optical amplifier in line with the transmission fiber and pumped by continuous wave optical power source can simultaneously amplify multiple wavelengths makes wavelength division multiplexing not only economical viable but also economical valuable. It is worth to mention that, such functionality is done with very high efficiency and, without causing any mixing or distortion between the signals being carried on the different amplified wavelengths. Moreover, the fiber amplifier can provide amplification for signals being carried on the wavelengths that have essentially arbitrarily bit rates. This is an enormously important and valuable feature of optical amplifiers that enables the ability to upgrade optical transmission systems to higher per wavelength bit rates without the need to replace amplifiers.

Along with mentioned ideas and driven by analogies to microwave systems, early researchers demonstrated basic optical switches that when connected to a fiber

could, under electrical control, dynamically switch out (drop) or switch in (add) a particular wavelength onto the fiber while leaving other wavelengths on the fiber unaltered. The research on optical switching technology received significant interest and activity in the late 1980s and early 1990s. It is one of the most important technologies that underpin today's optical networks. In general, optical switches are able to switch the path of the information carried by a particular wavelength in optical domain. In their simplest implementation, an optical switch is a wavelength add/drop multiplexer. Under electrical control, this device is able to switch a particular wavelength onto or off a fiber while leaving unaffected all other wavelengths on the fiber. More complex version of optical switches is the Optical Cross Connect (OXC) switch fabric, which uses a switching matrix to switch a particular wavelength from one of N input fiber routes to any of N output fiber routes (e.g. Reconfigurable Optical Add/Drop Multiplexers (ROADMs) [19]). Typically, this involves a combination of wavelength de-multiplexing, optical space switching, and wavelength multiplexing.

2.2 Optical amplifiers

With the development of optical amplifiers in the 80's and their first utilization in the 90's, the amplification process started to be realized exclusively in the optical domain and became transparent to the bit rate and modulation format [3]. Also, optical amplifiers became popular in WDM networks because they operate in a wide optical bandwidth and can amplify various channels simultaneously.

However, optical amplifiers are not perfect. Erbium doped fiber amplifiers, for example, introduce high noise levels (amplified spontaneous emission, ASE) to the optical signal. This noise is accumulated through cascades of optical amplifiers, causing OSNR reduction. Other amplifiers, like distributed Raman amplifiers, are expensive because they require high pump power to amplify the signal. This section describes the main optical amplifier technologies (EDF and Raman) and how their performance is evaluated.

2.2.1 Optical amplifiers technologies

Erbium doped fiber amplifier

The EDFA is constituted by a segment of erbium-ion (Er^{3+}) doped optical fiber (EDF). Figure 2.1 presents a typical schematic of the EDFA [20]. For a better energy transfer efficiency between the pump power and the signal, this fiber is pumped with lasers at 980 or 1480 nm [3]. At the input of the EDF, an optical coupler is used

to gather both pump power and signal power and an isolator is placed to prevent the ASE generated in the EDF during the amplification from returning to previous devices of the optical network and creating disturbances. At the output of the EDF, a splitter can be used to separate the signal from residual pump power and another isolator is used to prevent reflections or signals created by other devices of the optical network from interfering in the amplification process.

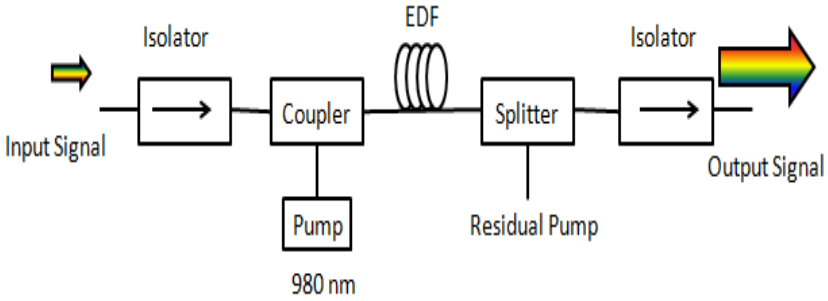

Figure 2.1: EDFA schematic.

To understand how the pump power amplifies the signal in the EDFA, it is necessary to observe the energy levels of erbium ions in silica [20]. In fact these energy levels are subdivided in various levels that constitute energy bands. These energy bands are important since they increase the number of wavelengths that can be amplified.

The EDFA operation principle is based on a stimulated emission process among three energy bands that are presented in Figure 2.2. In fact, the erbium ions presents many more energy bands in silica. The bands illustrated in Figure 2.2 only represents the useful bands for amplification. The pump power can amplify the frequencies that satisfy a difference of energy of $\Delta E = hf_c$, where ΔE is the difference of energy between the E2 and E1 energy bands and f_c the frequency of the signal to be amplified. For erbium ions in silica, the amplified signal wavelength band is situated between 1530 and 1565 nm which is also a low signal attenuation band in SSMFs used in communications systems (C band of the International Telecommunication Union grid). At the thermal equilibrium, the electron population of levels E1, E2, E3 presents the following relation: $N1 > N2 > N3$, where Ni, $i \in \{1, 2, 3\}$, is the electron population at the Ei level.

For example, by amplifying the signal with a 980 nm laser, the population inversion $N2 > N1$ is obtained after the combination of one absorption and one spontaneous emission. Electrons present at the E1 level absorb the pump photons and their energy level transits from E1 to E3. Then, these electrons at the energy level E3 decrease in energy through a non-radiative spontaneous emission and reach the level E2 with a lifetime of approximately 1 μs. The spontaneous emission from the E2 to the E1 energy state presents a lifetime of 10 ms which is much higher than the previous one. For this

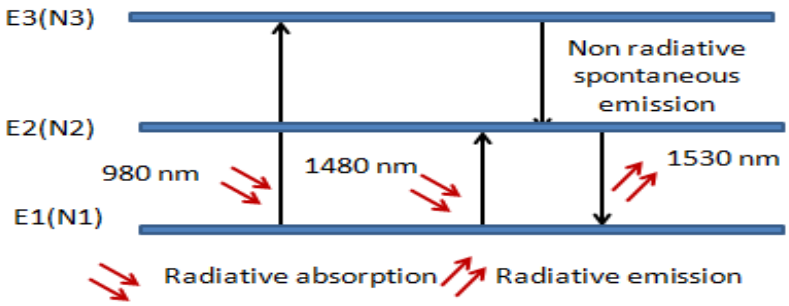

Figure 2.2: Energy bands of erbium ions in silica.

reason, the E2 energy level is metastable and is more populated than the E1 level and there is a population inversion [20].

Raman amplifiers

Raman amplification occurs thanks to stimulated Raman scattering that is a nonlinear effect [5]. During Raman scattering, light incident on a medium is converted to a lower frequency. This is shown in Figure 2.3. A pump photon ν_p excites a molecule up to a virtual level (non-resonant state). The molecule quickly decays to a lower energy level emitting a signal photon ν_s in the process. The difference in energy between the pump and signal photons is dissipated as molecular vibrations in the host material. These vibrational levels determine the frequency shift and shape of the Raman gain curve. Due to the amorphous nature of silica, the Raman gain curve is fairly broad in optical fibers. Figure 2.4 shows the Raman gain spectrum for two types of optical fibers. The frequency (or wavelength) difference between the pump and and the signal photon ($\nu_p - \nu_s$) is called Stokes shift.

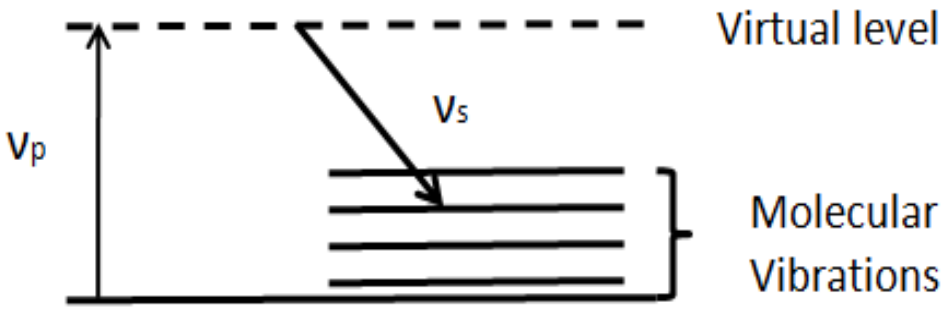

Figure 2.3: Raman scattering effect (source: Headley and Agrawal [5]).

For high enough pump powers, the scattered light can grow rapidly with most of the pump energy converted into scattered light. This process is called stimulated

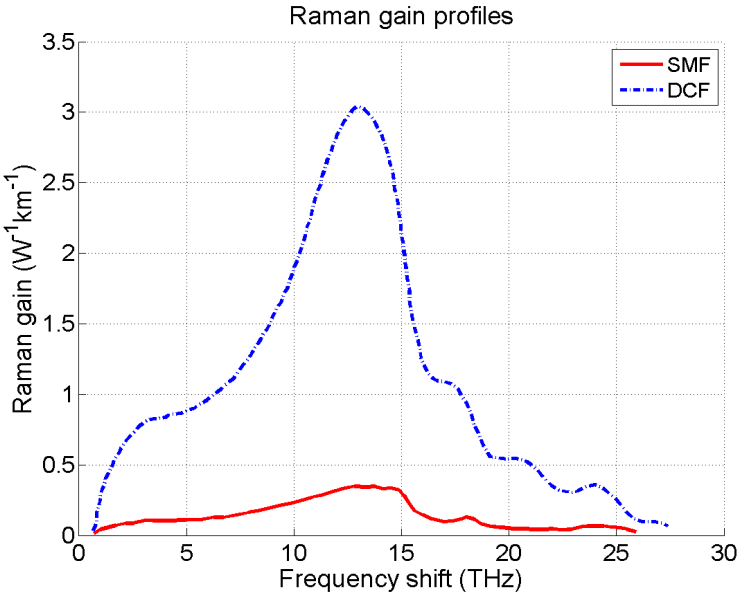

Figure 2.4: Raman gain profiles for a 1510 nm pump in two different fiber types: single mode fiber (SMF) and dispersion compensating fiber (DCF) (source: Headley and Agrawal [5]).

Raman scattering (SRS) and is the gain mechanism in Raman amplification. This mechanism counts three important points:

- SRS can occur in any fiber;
- Since the pump photon is excited to a virtual level, Raman gain can occur at any signal wavelength by proper choice of the pump wavelength;
- The Raman gain process is very fast.

This differs from the EDFA where:

- An EDF is required;
- The pump and signal wavelengths are determined by the resonant levels of erbium ions;
- The transfer of energy is much slower.

Further discussions about differences between the EDFA and the distributed Raman amplifier are presented in the next section.

There are two different types of Raman amplifiers: the lumped Raman amplifier (LRA) and the distributed Raman amplifier (DRA). Figure 2.5 presents a possible configuration for the lumped Raman amplifier. The pump power traveling in the same

direction as the signal is called co-propagating or forward pump, and the pump traveling in the opposite direction is called counter-propagating or backward pump. An interesting gain medium for the LRA is the DCF fiber. The DCF fiber is advantageous in the LRA for two reasons:

- For being highly nonlinear, the DCF presents a reasonable pump power conversion efficiency as seen in Figure 2.4 (this pump power conversion being lower than for the EDFA case but higher than for the DRA case); as a results, reasonable pump powers and only a few kilometers of DCF are sufficient to achieve high gains (< 5 km tipically);
- By using correctly the DFC at the amplifier plant, the nonlinear effects that occur in the transmission fiber can be compensated, which is convenient in coherent communication systems [21].

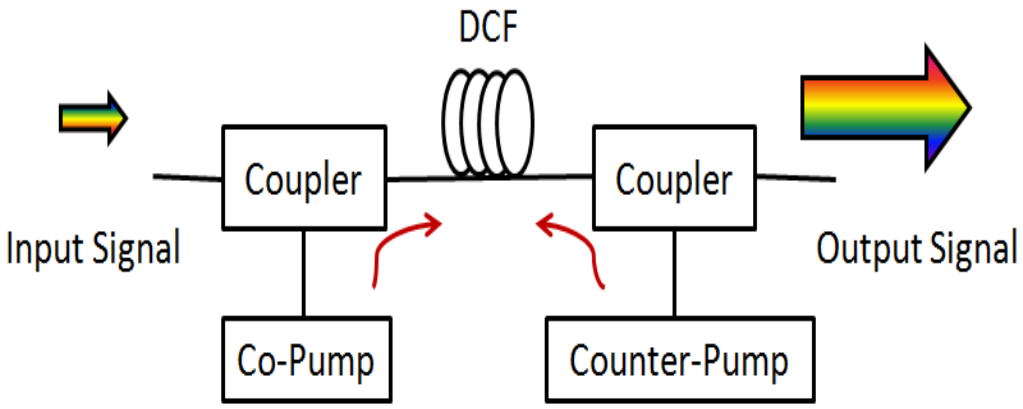

Figure 2.5: Lumped Raman amplifier with a DCF.

The main drawback with the LRA is its high noise figure due to the concentrated amplification [5]. This is not the case with the DRA amplifier.

Figure 2.6 presents a typical configuration for the DRA. In the co-propagating Raman amplifier (Figure 2.6(a)), the pump power travels in the same direction as the signal. In the counter-propagating Raman amplifier, Figure 2.6(b), the pump power travels in the opposite direction to the signal. With both co- and counter propagating configurations, the amplification occurs in the proper transmission fibers for many kilometers (typically a dozen). This makes the control of the amplifier in the automatic gain control mode difficult (cf. Chapter 3 and Section 4.1). Another drawback is that it requires high pump power to amplify the signal.

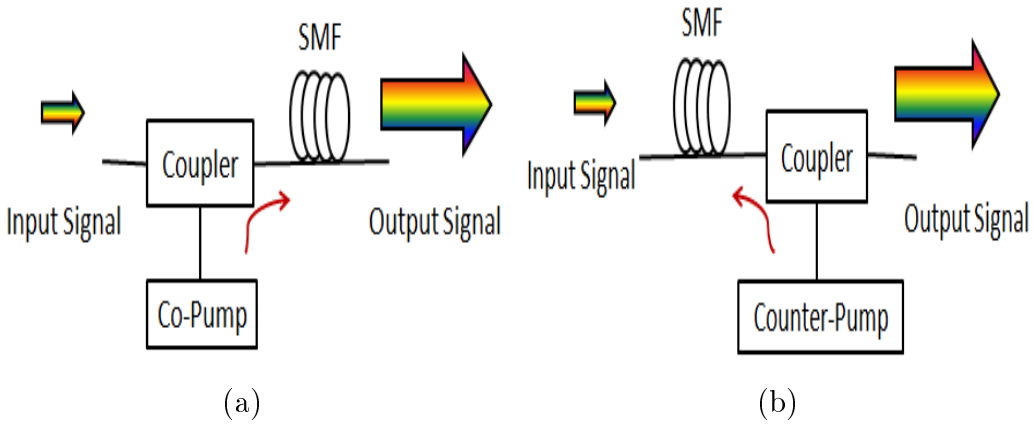

Figure 2.6: Typical schematics of distributed Raman amplifiers: (a) co-propagating DRA; (b) counter-propagating DRA.

Comparisons between the EDFA and the DRA technologies

A comparison between the performance of the EDFA and the DRA is summarized in Table 2.1. The main differences are the following:

- The EDFA pump laser wavelength if fixed and amplify a defined spectrum bandwidth whereas, with the DRA, the pump laser wavelength is chosen depending of the desired amplification optical bandwidth;
- The DRA amplifier requires higher pump power than that of the EDFA for equal optical gain; therefore, the DRA is more expensive than the EDFA [22];
- By combining pump lasers at different wavelength the DRA can amplify a wide optical bandwidth whereas, for the EDFA case, the amplification bandwidth remains the same;
- By combining pump lasers at different wavelength and by controlling their power appropriately the gain flatness of the DRA can be significantly improved [23] whereas, for the EDFA case, the only way to improve the gain flatness is to use a gain flattening filter (GFF) that decreases the OSRN [24];
- The noise figure of the EDFA is higher than for the DRA case;
- The time constant of Raman amplification is very low so the transient effects are negligible and this is not the case for the EDFA [25].

Table 2.1: Comparisons between the EDFA and the DRA.

Property	EDFA	DRA
Pump wavelength	980 nm or 1480 nm	100 nm lower than the signal at gain peak
Pump power	$>$ 10 mW	$>$ 100 mW
Power dissipation	low	high
Amplification band	1530-1565 nm	1280-1650 nm
Bandwidth	30 nm	$>$ 100 nm
Gain	$<$40 dB	$<$25 dB
Noise figure	$\sim$ 5 dB	$<$3 dB
Gain flatness	GFF is required for long haul application	pump wavelength dependence
Time constant	10^{-2} s	10^{-15} s
Cost	medium	high

As a conclusion, even if the EDFA has a lower cost and a higher pump conversion efficiency, Raman amplifiers have gained interest after the 2000s because they enable a large amplification bandwidth which is an asset in current optical networks that must support bandwidth-hungry services and applications. The DRA has an advantage over the LRA in relation to the noise figure. However, this distributed amplification makes its control in the AGC mode (defined in the next section) more difficult (as presented in Chapter 3 and Section 4.1).

2.2.2 Characterization of optical amplifiers

Optical networks have evolved from static to dynamic scenarios. Nowadays the channel load can vary in an unpredictable way. Consequently optical amplifiers must be able to operate in a signal input power range that corresponds to the variation of the channel load. Another necessity is to operate at different gains in order to compensate the total optical output power of the amplifier for variations of the input power caused by dynamic switch out (drop) or switch in (add) of optical channels.

The input power range and the gain range define the operating region of the optical amplifier. The good performance of the amplifier that is only garanteed in this region can be plot in an amplifier power masks [26]. Figure 2.7 shows how these amplifier power masks are built. On the horizontal and vertical axis the input power (P_{in}) and the output power (P_{out}) of the amplifier are represented, respectively. Each colored point inside the power mask, associated with the colored bar on its right, gives the performance of the amplifier at the corresponding operation point (referenced by its input power and target gain) in relation to the parameter at study indicated in the title of the figure. The

Max, *Mean* and *Min* values, which correspond to the maximum, mean and minimum values of the parameter, respectively, are indicated on the top left of the amplifier power mask.

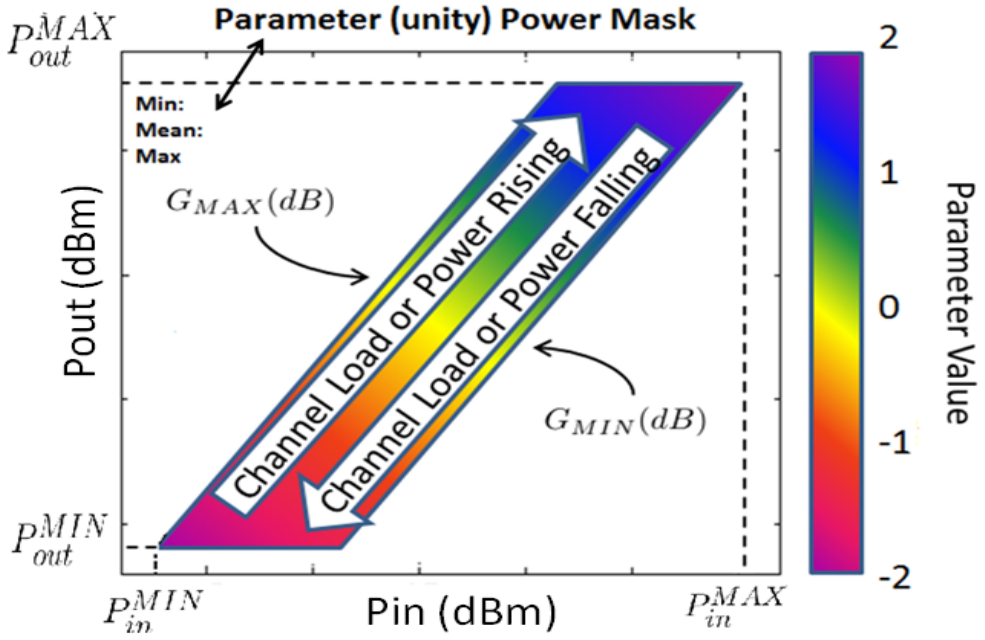

Figure 2.7: Amplifier power mask.

Important relations can be deduced from the power mask:

$$P_{\text{out}}^{\text{MIN}} = P_{\text{in}}^{\text{MIN}} + G_{\text{MAX}} \tag{2.1a}$$

$$P_{\text{in}}^{\text{MAX}} = P_{\text{out}}^{\text{MAX}} - G_{\text{MIN}} \tag{2.1b}$$

where $P_{\text{out}}^{\text{MIN}}$, $P_{\text{out}}^{\text{MAX}}$, $P_{\text{in}}^{\text{MIN}}$ and $P_{\text{in}}^{\text{MAX}}$ are the minimum and maximum values of P_{out} and P_{in} (in dBm), respectively, G_{MIN} and G_{MAX} are the minimum and maximum gains (in dB), respectively. For example, if the amplifiers performance is guaranteed between the minimum output power at the maximum gain $P_{\text{out}}^{\text{MIN}} = -1$ dBm and maximum input power $P_{\text{in}}^{\text{MAX}} = 7$ dBm and can operates in a gain range varying from $G_{\text{MIN}} = 14$ dB to $G_{\text{MAX}} = 24$ dB, the additional values of $P_{\text{out}}^{\text{MAX}}$ and $P_{\text{in}}^{\text{MIN}}$ calculated to complete the definition of the power mask region are the following:

$$P_{\text{out}}^{\text{MAX}} = 7 + 14 = 21 \text{ dBm}$$

$$P_{\text{in}}^{\text{MIN}} = -1 - 24 = -25 \text{ dBm}$$

The dynamic range (DR, in dB) of the amplifier is defined as the range between the smallest and highest output powers:

$$DR = P_{\text{out}}^{\text{MAX}} - P_{\text{out}}^{\text{MIN}}. \tag{2.2}$$

The amplifier can be optically characterized for several parameters. The most relevant ones for this work are the automatic gain control accuracy (AGC accuracy), the gain flatness and the noise figure.

AGC accuracy

When the amplifier operates in the AGC mode, the control parameter to be optimized is the gain of the amplifier. This gain (G, in dB) is defined as the difference between the total output and input powers of the amplifier:

$$G = P_{out} - P_{in} \tag{2.3}$$

When setting a target gain (TG, in dB) for the amplifier, the real output power (RP_{out}, in dBm) is not always $RP_{out} = P_{in} + TG$, since there may be an error in the gain control. Therefore, new relations are defined:

$$TP_{out} = P_{in} + TG \tag{2.4a}$$

$$RP_{out} = P_{in} + RG \tag{2.4b}$$

where TP_{out} and RP_{out} are the target and real total output powers, respectively, TG and RG are the target and real gains, respectively.

With this consideration, the AGC error of the amplifiers (in dB) is defined as follows:

$$AGC_{error} = |TP_{out} - RP_{out}| \tag{2.5}$$

Gain flatness

The amplification gain curve of the amplifier is not flat within the optical signal bandwidth. As a consequence, some channels are more amplified than others. To evaluate the gain flatness of the amplifier, the ripple (*ripple*, in dB) can be defined. By

considering that at the input of the amplifier all the channels are equalized (i.e., same optical power), the ripple, at a specific operation point of the amplifier, is the maximum channels power difference at the output of the amplifier.

Noise Figure

The noise figure (NF) of an amplifier is the difference between the SNR of the input signal and the SNR of the output signal, for a result in dB (both SNRs are obtained after measuring the optical power with a photodetector). It is a measure of how much the amplifier degrades the signal. Appendix A presents in detail the noise figure calculation for distributed Raman amplifiers [5].

Chapter 3

Automatic Gain control of optical amplifiers

To cope with dynamic channel switching (add and drop) occurring in optical networks, optical amplifiers have to operate in automatic gain control mode in order to compensate the total output optical power for variations of the input power. Depending on the amplifier topology, different gain control schemes can be implemented . This chapter shows the difference of AGC between concentrated and distributed amplifiers. Then, the gain control of distributed counter-propagating Raman amplifiers that will be used in this Masters dissertation is presented in details.

3.1 Concentrated amplifiers

In concentrated amplifiers, the amplification occurs in short fiber lengths (in general, a few meters of erbium-doped fiber for the EDFA and a few hundred meters of DCF for the LRA). Therefore, these amplifiers can be encapsulated in field installations and the measurement of their input and output power is easy. Figure 3.1 illustrates a possible EDFA gain control using a proportional-integral (PI) controller [27]. In this loop control, the input and output power levels of the amplifier are measured to calculate the real gain of the amplifier. The gain error, which is the difference between the target and real gain, is calculated and feeds a PI controller that returns a pump power adjustment to enhance the gain accuracy. After a few iterations of this process, the real gain converges to the target gain.

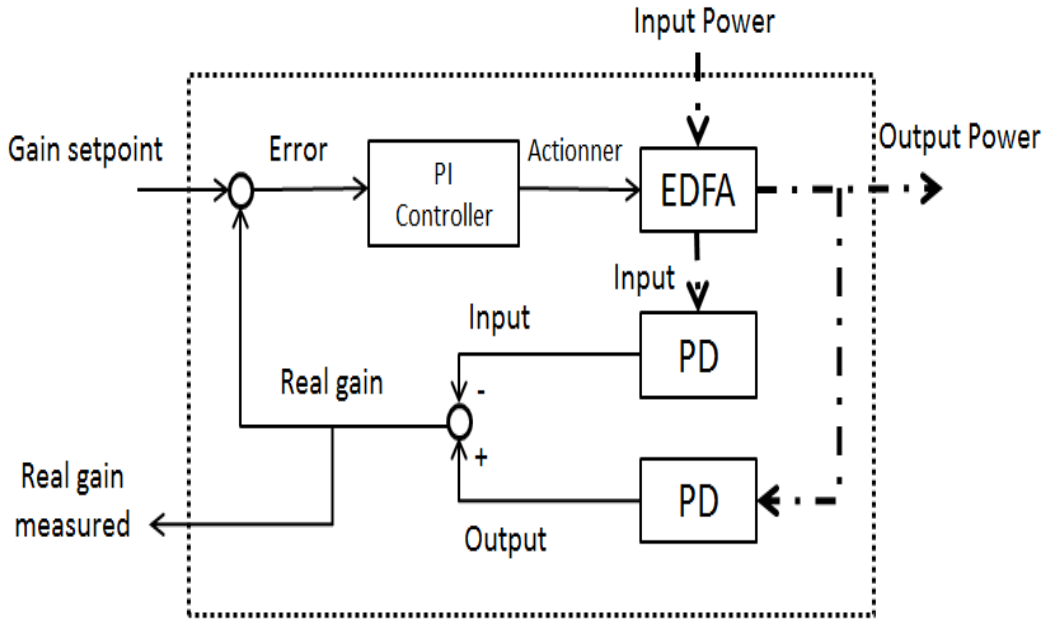

Figure 3.1: EDFA AGC with a PI controller.

3.2 Distributed amplifiers

In distributed Raman amplifiers, the pump power used for the amplification is sent directly into the transmission fiber.

On the one hand, with the co-propagating Raman, Figure 2.6(a), the pump power used for the amplification is sent in the same direction as the signal propagation. For gain control, the input and output powers would be the total optical power at the entry of the coupler and at the end of the SMF respectively.

On the other hand, with the counter-propagating Raman, Figure 2.6(b), the pump power used for the amplification is sent in the opposite direction of the signal propagation. For gain control, the input and output powers would be the total launch power into the SMF and the total output power after the coupler, respectively.

The difficulty to control distributed Raman amplifiers in the AGC mode can be understood by formulating the following observation.

At the co-propagating (counter-propagating) Raman amplifier plant alone, only the input (output) power is available since distributed amplifiers are not encapsulated devices. As a consequence, the real-time gain of the amplifier cannot be known for gain control. This problem would be solved if optical networks used centralized controls where the information of the total powers at each device and node would be accessible. These optical networks are mainly laboratorial prototypes and most of the field installations do not have a centralized control.

3.3 Distributed counter-propagating Raman amplifier

Precedently, optical amplifiers and their gain control were compared. From now, this work will focus on how to realize and optimize the distributed Raman counter-propagating amplifier AGC.

3.3.1 On-off gain

Section 3.3 showed that there is no access to the input power of the counter-popagating DRA and thus to the real gain of the amplifier. To overcome this limitation, another gain needs to be used: the on-off gain [5]. The on-off gain corresponds to the difference of output power of the amplifier with and without the pump lasers turned on, respectively. That is:

$$G_{on-off} = P_{on} - P_{off} \tag{3.1}$$

where G_{on-off} is the on-off gain (in dB) and P_{on} and P_{off} are the total output power of the amplifier with the pump lasers turned on and off (in dBm), respectively. As a consequence, all previously defined relations involving P_{in} and P_{out} in Section 2.2.2 can be written again substituting P_{in} (P_{out}) by P_{off} (P_{on}) and then $G = G_{on-off}$.

A more precise schematic of the classical counter-propagating DRA is shown in Figure 3.2. The optical signal is launched into a single mode fiber (SMF) with an unknown total optical power P_{launch}. The pump combiner (PC) couples the lasers pump power in the wavelengths λ_i and with nominal power of $P_{\text{nom-}i}$, $i \in \{1, .., n\}$ where n is the number of pump lasers. This pump power is coupled into the transmission fiber, amplifying the optical signal in counter-propagation. A photodetector (PD) receives a fraction of the total output power of the amplifier for the gain control. The real-time pump power P_{pump} (in mW) and the transmission fiber total attenuation $Loss$ (in dB) are also defined.

3.3.2 On-off gain control implementation

The DRA AGC is an open loop system where the pump power is adjusted depending on the measured total output power and the target gain. This open loop is illustrated in Figure 3.3. When operating, the pump lasers of the DRA cannot be turned off to measure P_{off} because this would strongly disturb the optical traffic. Therefore, the real-time on-off gain of the amplifier cannot be known and the pump power adjustments for AGC accuracy cannot be processed like in the EDFA case (cf. Section 3.1). A solution to this problem consists in estimating P_{off} from P_{on} and the target gain and to find a

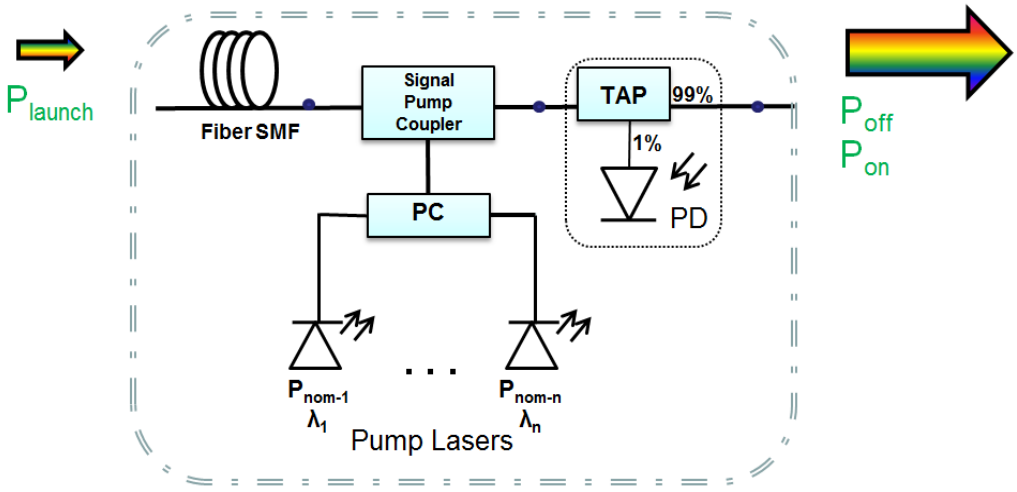

Figure 3.2: Distributed counter-propagating Raman amplifier.

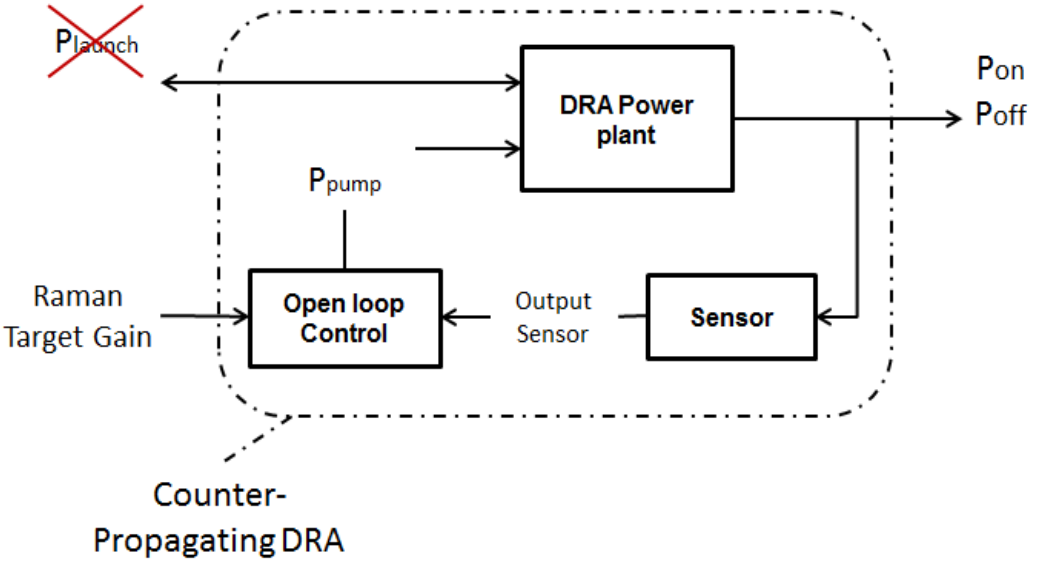

Figure 3.3: Gain control system of the DRA.

relation that maps, for each P_{off} and target gain, the pump power that must be set. This relation is given by the gain control polynomials (GCPs).

GCPs generation procedure

GCPs are required to adjust the pump power of the DRA for each target gain, depending on the actual P_{off}. This adjustment must be done for all the operating points of the amplifier that are defined by the amplifier power mask limits (cf. Section 2.2.2). In this Masters dissertation, the amplifier power mask limits that are appropriate for the study of the DRA performance [28] are the following:

$$P_{\text{on}}^{\text{MIN}} = -10 \text{ dBm}$$

$$P_{\text{off}}^{\text{MAX}} = 0 \text{ dBm}$$

$$G_{\text{MIN}} = 2 \text{ dB}$$

$$G_{\text{MAX}} = 12 \text{ dB}$$

$$P_{\text{on}}^{\text{MAX}} = 0 + 2 = 2 \text{ dBm}$$

$$P_{\text{off}}^{\text{MIN}} = -10 - 12 = -22 \text{ dBm}$$

The GCPs generation procedure consists in storing the DRA response varying the P_{launch} and P_{pump} parameters according to the following stages:

- First: in this stage, the total launch power P_{launch} is varied in 45 steps with a granularity of 0.5 dB in order to vary $P_{\text{off}} = P_{\text{launch}} - Loss$ from 0 to −22 dBm.
- Second: this stage is executed for each step of the first stage and consists in varying the pump power of the amplifier in 46 steps with an exponential (base 10) granularity between the minimum pump power (0 mW) and the maximum pump power (360 mW).

For these 2070 iterations, the values of P_{on}, P_{off}, P_{pump} and $G_{\text{on/off}}$ are stored. Then, the data is organized and the coefficients of 11 fifth-order polynomials ($G_{\text{MAX}} - G_{\text{MIN}} + 1 = 11$) are generated to relate, for each target gain, the P_{off} and P_{pump} powers:

$$\begin{aligned} P_{pump}^{TG_X}(P_{off}) = a_5 P_{off}^5 + a_4 P_{off}^4 + a_3 P_{off}^3 \\ + a_2 P_{off}^2 + a_1 P_{off} + a_o, \end{aligned} \tag{3.2}$$

where $P_{\text{pump}}^{\text{TG}_X}(P_{\text{off}})$ is the pump power that must be set to provide the target on-off gain X (in dB) at the current P_{off} and a_0, a_1, a_2, a_3, a_4, a_5 are the fifth-order polynomial regression coefficients obtained.

On-off gain control definition

The DRA on-off gain control is based on the use of the GCPs previously generated. Its implementation is illustrated in the flowchart of Figure 3.4 and is presented in [15] and [28] .

During the on-off gain control, P_{off} is estimated from P_{on} and the set gain by calculating $P_{\text{off}} = P_{\text{on}} - TG_X$. With this estimation and the GCPs, it is possible to calculate the P_{pump} power that would be necessary to obtain the set gain. If P_{pump}

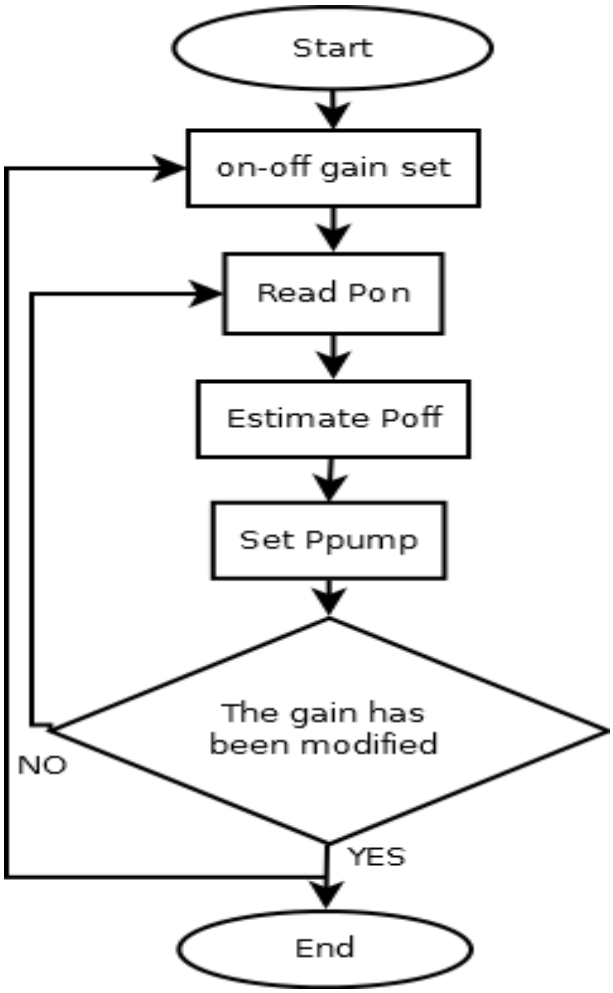

Figure 3.4: On-off gain control of the DRA.

does not provide the desired gain, its value will be corrected in the next iteration after re-estimating P_{off}. Such iterative correction is done until converging to the gain set or receiving another target gain instruction.

Example: Suppose that the current amplifier operation state is:

$$P_{off} = \text{ -10 dBm (value that cannot be measured);}$$
$$P_{pump} = \text{ 70 mW;}$$
$$P_{on} = \text{ -6 dBm;}$$
$$TG = \text{ 4 dB.}$$

Then, the DRA target gain is modified from 4 to 10 dB. At each iteration, that is one loop in the Figure 3.4 flowchart, the DRA evolves to a new state where the real gain of the amplifier tends to reach the 10 dB target gain. An example of how the DRA could evolve is presented in Table 3.1.

At iteration 1, the gain is modified from 4 to 10 dB. P_{on} and RG remain the

Table 3.1: Example of gain control evolution of the DRA.

Iteration	TG	P_{on}	RG	P_{off} estimated	P_{pump}
Initial state	4	-6	4	-10	70
1	10	-6	4	-16	150
2	10	-2	8	-12	160
3	10	0	10	-10	165

same as in the initial state, since the pump power has not yet changed. P_{off} is estimated from P_{on} and the target gain: $P_{off} = P_{on} - TG_{10} = -6 - 10 = -16$ dBm. With the estimated P_{off} and the target gain, the pump power to be set can be calculated with Equation 3.2.

At iteration 2, the same procedure is repeated.

At iteration 3, the real gain is equal to the target gain and the algorithm has converged so the pump power will remains the same in the next iterations. New adjustments of the pump power will be necessary if a new target gain is configured or if P_{off} is varied due to channel load variations or transmission fiber degradations.

Chapter 4

Field calibration procedure for counter-propagating DRAs

4.1 In-field operational issues with DRAs and motivation of this work

The GCPs generation, presented in Section 3.3.2, is usually realized with the transmission fiber in the laboratory. In fact, the characteristics of the transmission fiber (e.g., attenuation at the pump power and signal wavelength, geometry, chemical composition) have an influence on the Raman gain [6]. As a result, there are two main operational issues in the deployment of DRAs.

On the one hand, higher attenuation of the transmission line due to fiber aging or discrete loss points (e.g., dirty or faulty connectors and splices, sharp bends and other stress points) occurring close to the DRA can severely decrease the available pump power for the Raman amplification, and thus the achievable Raman gain.

On the other hand, back-reflections, often associated with discrete loss points at connectors or splices, can occur in the transmission fiber. In these back-reflections, part of the pump energy propagating along the line will return to the pump lasers source. A high level of back-reflection can degrade the performance of the lasers, and thus decrease the available pump power for Raman amplification.

To overcome these issues, an in-field calibration procedure of the DRA is needed in its installation or whenever the characteristics of the field transmission fiber are modified to ensure accurate AGC. This calibration could be the regeneration of the GCPs in the same way that they are generated in the laboratory (cf. Section 3.3.2). Two notable drawbacks prevent this in-field GCPs regeneration:

- The traffic would be stopped during hours; this is not viable since the traffic cannot

be blocked for a long time due to operators' requirements;

- A centralized control would be necessary; this centralized control would be able to vary P_{launch} in steps of 0.5 dB modifying the gain of a previous amplifier of the optical link or attenuating its output power; usually, it is not possible to control P_{launch}.

The field calibration procedure proposed in this Masters dissertation is much faster than this GCPs regeneration since it requires only a few minutes of processing. Furthermore, it does not need a centralized control.

The calibration procedure is based on the relation between the different generated GCPs (cf. Section 3.3.2). In the next section, a study of the GCPs properties is reviewed. Then, the in-field calibration procedure is presented.

4.2 Study of the GCPs properties

The GCPs generated according to the procedure defined in Section 3.3.2 and under the simulation setup that will be described in Section 5.1 are illustrated in Figure 4.1(a). The simulation setup is not detailed in this chapter because the concepts described below are general for DRAs and similar results would be obtained with another simulation setup. Each GCP corresponds to a target gain of the amplifier. According to the amplifier power mask limits defined in Section 3.3.2, the P_{off} power range domain of each gain polynomial is defined as:

$$\mathcal{D}_{\text{TG}_\text{X}} = [P_{\text{on}}^{\text{MIN}} - TG_X \, , \, P_{\text{on}}^{\text{MAX}} - TG_X] = [-10 - TG_X \, , \, 2 - TG_X], \tag{4.1}$$

Fig. 4.1(a) shows the GCPs plot in their definition domain. Accounting for the similar shapes of the GCPs, it is possible to formulate the following hypothesis:

Hypothesis 1: There is a linear relation between the gain variation (ΔTG) and the pump power variation (ΔP_{pump}) between two GCPs. That is, $\Delta P_{\text{pump}} = k\Delta TG$, where k is a linear coefficient. This linear variation is independent of P_{off}.

To validate Hypothesis 1, it is possible to proceed as follows:

- The mean of the pump power difference $\Delta P_{\text{pump}}^{\text{TG}_X,\text{TG}_{X+1}}$ between each successive GCP over the intersection of their definition domains $I_{TG_X,TG_{X+1}} = \mathcal{D}_{\text{TG}_X} \cap \mathcal{D}_{\text{TG}_{X+1}}$ is calculated:

$$\Delta P_{\text{pump}}^{\text{TG}_X,\text{TG}_{X+1}} = \frac{1}{DR-2} \sum_{P_{\text{off}} \in I_{TG_X,TG_{X+1}}} P_{\text{pump}}^{\text{TG}_{X+1}}(P_{\text{off}}) - P_{\text{pump}}^{\text{TG}_X}(P_{\text{off}}), \tag{4.2}$$

where $DR-2$ is the number of integer P_{off} in $I_{TG_X,TGX+1}$, when considering a P_{off} and gain granularity of 1 dB (cf. Sections 3.3.2 and 2.2.2).

- The GCPs of successive target gains TG_X and TG_{X+1} dB for which the $\Delta P_{\text{pump}}^{\text{TG}_X,\text{TG}_{X+1}}$ value is the closest to the mean of all the $\Delta P_{\text{pump}}^{\text{TG}_X,\text{TG}_{X+1}}$ values calculated for all the successive gains are chosen as the best fitted GCPs. In the case presented in Fig. 4.1(a), these GCPs are the polynomials of target gains 4 and 5 dB.

- Taking as a reference the 4 dB gain polynomial, the $\Delta P_{\text{pump}}^{\text{TG}_4,\text{TG}_{4+U}}$ values, being $U \in \{-2,..,8\}$, are plotted as a function of the gain variation $\Delta TG = U$ dB in Figure 4.1(b). The linear approximation $\Delta P_{\text{pump}} = \Delta P_{\text{pump}}^{\text{TG}_4,\text{TG}_5} \Delta TG$ is also plotted in Figure 4.1(b).

- The difference between the two curves of Figure 4.1(b) is plotted in Figure 4.1(c) as a percentage of the maximum pump power used for the GCPs generation (205 mW).

- The standard deviation of the pump power difference between all the successive GCPs is calculated at each P_{off} and the results are plot in Fig. 4.1(d) (as a percentage of the previously mentioned maximum pump power).

Figures 4.1(a), (b) and (c) demonstrate that the pump power variation between two polynomials is, on average over the P_{off} power ranges, proportional to the gain difference between the same GCPs. Indeed, the real pump power variation in relation to the gain difference fits very well its linear approximation. Figure 4.1(d) shows that this linear dependency is nearly independent of P_{off} since the standard deviation of the pump power difference between successive polynomials as a percentage of the maximum pump power remains very low. As a conclusion, Hypothesis 1 holds and a good approximation of the linear coefficient k is $\Delta P_{\text{pump}}^{\text{TG}_4,\text{TG}_5}$, obtained with the best fitted successive GCPs of gains 4 and 5 dB.

Important remark: Hypothesis 1 was proved in a specific P_{off} range (between 0 dBm and -22 dBm) and for pump levels below 205 mW. This hypothesis may be questionable for other P_{off} values and for higher pump levels.

4.3 Proposed calibration procedure

The proposed in-field calibration procedure is based on Hypothesis 1 and consists in evaluating the pump power efficiency of the amplifier with the field transmission fiber and calculating, for each target gain, the pump power offset to be added to the pump power calculated by the GCPs. This is described in the following list of actions.

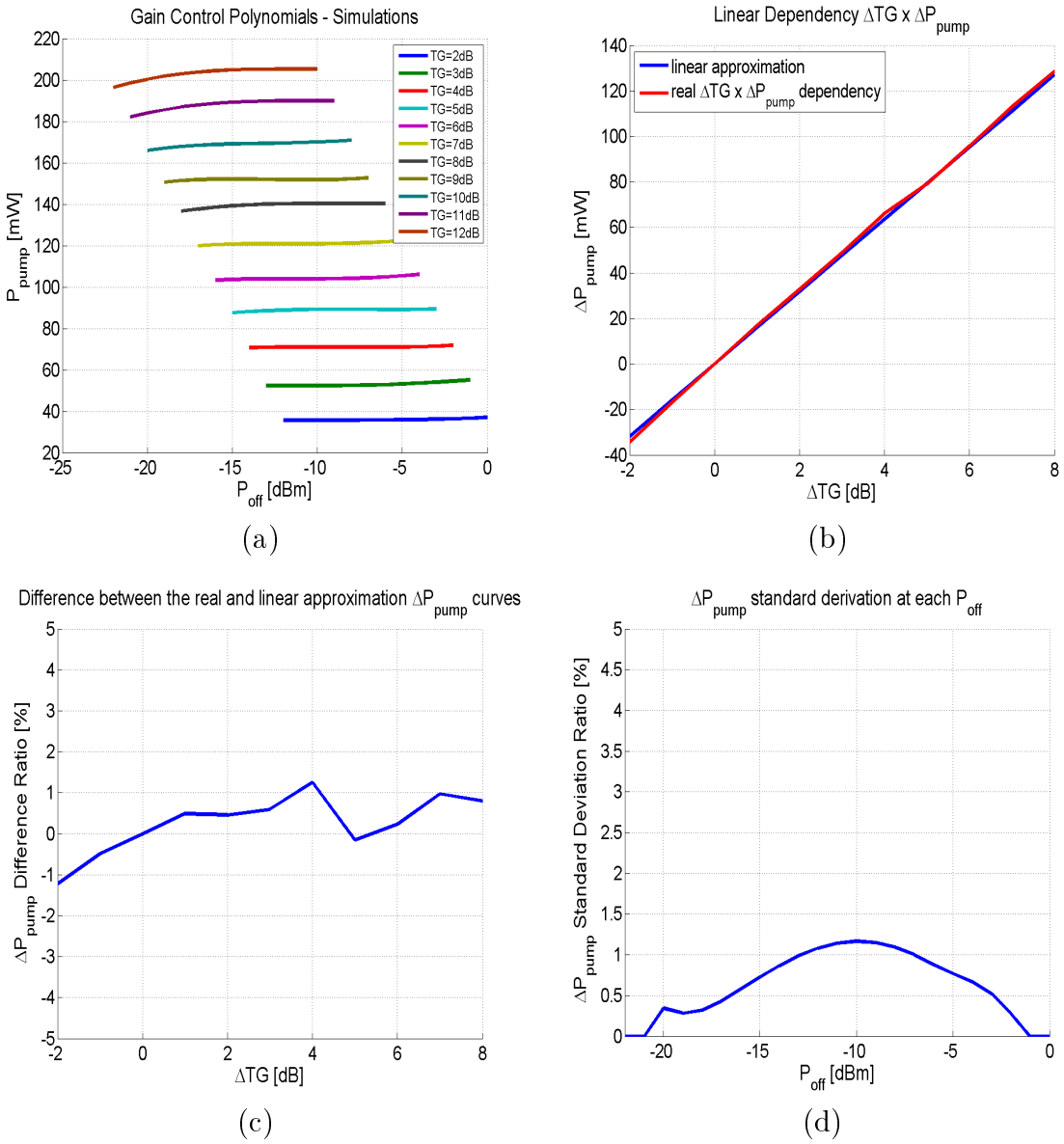

Figure 4.1: Polynomials study: (a) gain control polynomials generated, simulations; (b) ΔGx$\Delta Pump$ function and its linear approximation; (c) difference between the real and linear approximation curves of Figure 4.1(b) as a percentage of the maximum pump power (205 mW); (d) standard deviation pump power as a percentage of the maximum pump power (205 mW).

In-field DRAs calibration procedure:

1. Turn off the pump lasers. Measure and save P_{off}.

2. Turn on the pump lasers and set a target gain TG_X. Set the pump power $P_{\text{pump}}^{TG_X}$ calculated by the TG_X polynomial. Measure and save P_{on} for TG_X, $P_{\text{on}}^{TG_X}$. Repeat the same steps of this item with the target gain $TG_{X+1} = TG_X + 1\,\text{dB}$. Measure and save $P_{\text{on}}^{TG_{X+1}}$ and $P_{\text{pump}}^{TG_{X+1}}$. The target gains TG_X and TG_{X+1} are the gains of

the best fitted polynomials defined in Section 4.2.

3. Calculate and save the real gains RG_X and RG_{X+1} obtained when setting the target gains TG_X and TG_{X+1} respectively:

$$RG_X = P_{\text{on}}^{TG_X} - P_{\text{off}} \tag{4.3a}$$

$$RG_{X+1} = P_{\text{on}}^{TG_{X+1}} - P_{\text{off}} \tag{4.3b}$$

The $\Delta P_{\text{pump}}^{TG_{X,X+1}}$ power is defined:

$$\Delta P_{\text{pump}}^{TG_{X,X+1}} = P_{\text{pump}}^{TG_{X+1}} - P_{\text{pump}}^{TG_X} \tag{4.4}$$

4. Calculate and save the pump power variation necessary to increase the real gain of 1 dB, $\Delta P_{\text{pump}}^{RG+1}$, defined as follows:

$$\Delta P_{\text{pump}}^{RG+1} = \frac{\Delta P_{\text{pump}}^{TG_{X,X+1}}}{RG_{X+1} - RG_X} \tag{4.5}$$

It is important to note that this calculation is consistent with the assumption that Hypothesis 1 is true since the linearity between the pump power variation and the gain difference is used.

5. Add an offset, $offset_{GT_X}$, to the zero degree coefficient of the TG_X polynomial ($a_0^{TG_X}$):

$$offset_{TG_X} = (TG_X - RG_X)\Delta P_{\text{pump}}^{RG+1} \tag{4.6}$$

It is sufficient to add an offset to the polynomial in order to correct it because the linear variation implied by Hypothesis 1 is independent of P_{off} (only the zero degree coefficient of the polynomial needs to be corrected).

6. Add an offset, $offset_{TG_{X+k}}$, to the zero degree coefficients of all the others GCPs:

$$offset_{TG_{X+k}} = a_0^{TG_X} + offset_{TG_X} + k\Delta P_{\text{pump}}^{RG+1} - a_0^{TG_{X+k}} \tag{4.7}$$

with $k \in \mathbb{Z}$ and $a_0^{GT_{X+k}}$ the zero degree coefficient of the polynomial of gain $GT_{X+k} = GT_X + k\,\text{dB}$.

Example: Figure 4.2 show a calibration procedure example. The continuous lines represent the GCPs before calibration (B.C.). The dotted lines represent the GCPs after

calibration (A.C.). In this example, the gains of the best fitted polynomials are 3 and 4 dB.

Field calibration procedure:

1. The pump lasers are turned off and $P_{off} = -9$ dBm is measured;

2. The pump lasers are turned on and a first target gain $TG_3 = 3$ dB is configured. The pump power $P_{\text{pump}}^{TG_3} = 107$ mW is calculated by the TG_3 polynomial (point A). $P_{\text{on}}^{TG_3} = -6.4$ dBm is measured and saved. A second target gain $TG_4 = TG_3 + 1 = 4$ dB is configured. The pump power $P_{\text{pump}}^{TG_4} = 143$ mW is calculated by the TG_4 polynomial (point B). $P_{\text{on}}^{TG_4} = -5.56$ dBm is measured and saved.

3. The real gains RG_3 and RG_4 obtained when setting the target gains TG_3 and TG_4 are calculated and saved:

$$RG_3 = P_{\text{on}}^{TG_3} - P_{\text{off}} = -6.4 - (-9) = 2.6 \text{ dB} \tag{4.8a}$$

$$RG_4 = P_{\text{on}}^{TG_4} - P_{\text{off}} = -5.56 - (-9) = 3.44 \text{ dB} \tag{4.8b}$$

$\Delta P_{\text{pump}}^{TG_{X,X+1}}$ is calculated:

$$\Delta P_{\text{pump}}^{TG_{X,X+1}} = P_{\text{pump}}^{TG_4} - P_{\text{pump}}^{TG_3} = 143 - 107 = 36 \text{ mW} \tag{4.9}$$

4. The pump power variation necessary to increase the real gain of 1 dB, $\Delta P_{\text{pump}}^{RG+1}$ is calculated and saved:

$$\Delta P_{\text{pump}}^{RG+1} = \frac{\Delta P_{\text{pump}}^{TG_{3,4}}}{RG_3 - RG_4} = \frac{36}{3.44 - 2.6} = 42.9 \text{ mW} \tag{4.10}$$

5. An offset, $offset_{GT_3}$, is added to the zero degree coefficient of the TG_3 polynomial ($a_0^{TG_3}$):

$$offset_{TG_3} = (TG_3 - RG_3)\Delta P_{\text{pump}}^{RG+1} = (3 - 2.6)42.9 = 17.16 \text{ mW} \tag{4.11}$$

6. An offset, $offset_{TG_{3+k}}$, is added to the zero degree coefficients of all the others GCPs:

$$offset_{TG_{3+k}} = a_0^{TG_3} + offset_{TG_3} + k\Delta P_{\text{pump}}^{RG+1} - a_0^{TG_{3+k}} \tag{4.12}$$

with $k \in \mathbb{Z}$ and $a_0^{GT_{3+k}}$ the zero degree coefficient of the polynomial of gain $GT_{3+k} = GT_3 + k$ dB.

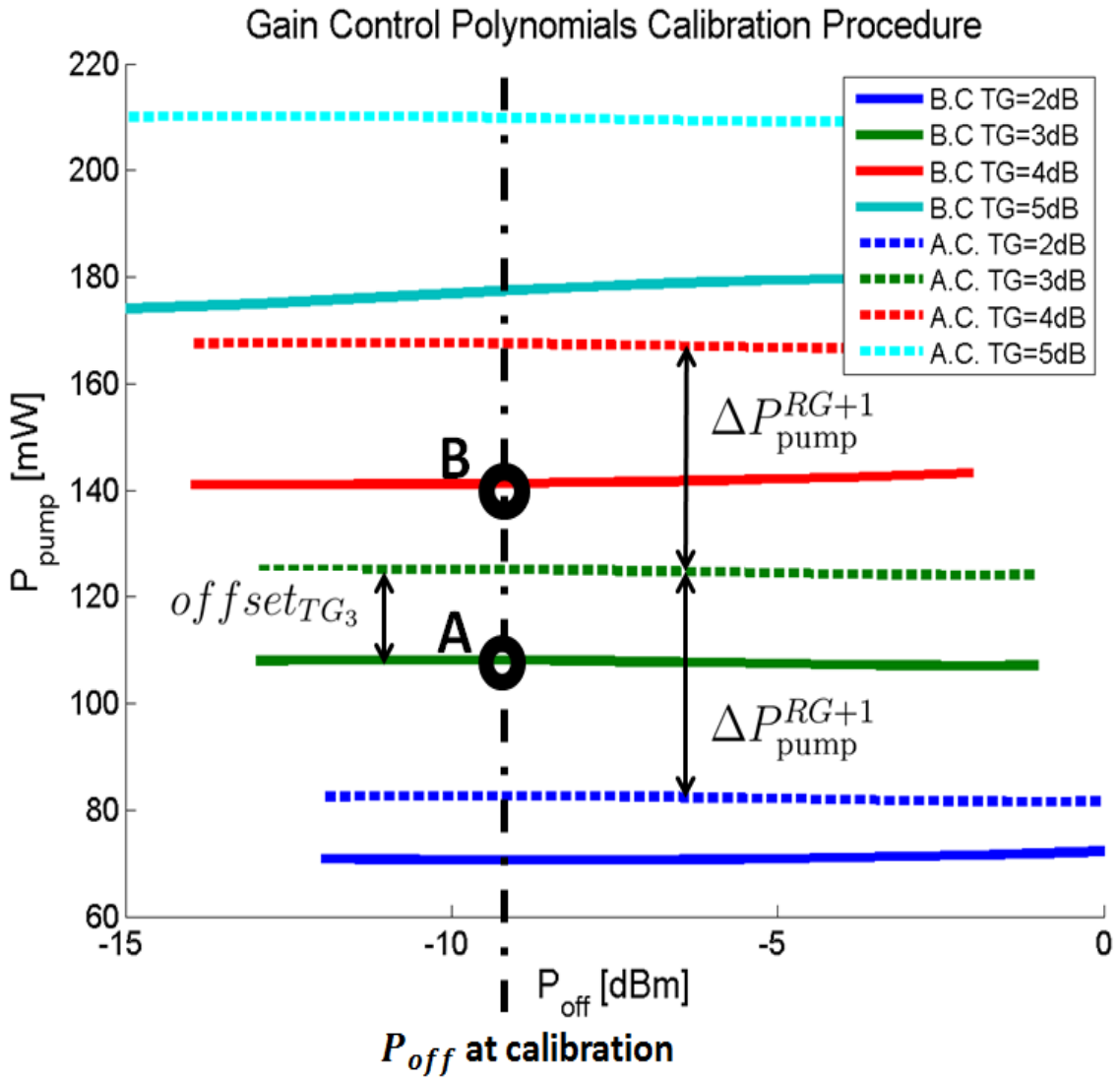

Figure 4.2: Field calibration example.

It is important to emphasize that the in-field calibration of the amplifier is realized at any P_{off}. This P_{off} depends on the channel loads and is not controllable. In the next chapter, which reports the simulation results, the amplifier performance in terms of AGC accuracy is evaluated for calibrations at different P_{off}.

Chapter 5

Simulation Results

5.1 Simulation setup

The simulations at study in this work were realized at CPqD Foundation. The Optisystem and MATLAB® softwares were used. The setup was arranged according to the schematic of the DRA presented in Figure 3.2.

The signal launch into the transmission fiber is composed of 40 continuous wave lasers with frequencies ranging from 192.1 to 196 THz (100 GHz of channel spacing). The transmission fiber length is 100 km. Two pump lasers are chosen for the Raman amplification in the 1425 and 1452 nm wavelengths. Both lasers have a nominal power of 360 mW and their power is controlled simultaneously to be the same. Therefore, when the pump power is specified, it corresponds to the pump power of only one laser. For example, if $P_{pump} = 200$ mW, it means that each laser power is 200 mW (the total pump power being in fact 400 mW).

5.2 Configurations studied

The performance of the in-field calibration is evaluated for transmission fibers of different attenuation profiles. These profiles are presented in Figure 5.1 (A_F is the attenuation profile of the fiber of index F, being $F \in \{0, .., 4\}$). The A_F profiles with $F \neq 0$ are obtained from the A_0 profile by adding an attenuation of $0.01F$ dB/km for all the wavelengths (to have a total attenuation of 1 dB over the whole transmission fiber of 100 km). These profiles of higher attenuation allow to evaluate the efficiency of the calibration procedure since the AGC will always be performed using the polynomials generated with the A_0 profile, when the real fiber profile is A_F, $F \in \{1, .., 4\}$. The polynomials presented in Figure 4.1(a) were generated with the A_0 profile.

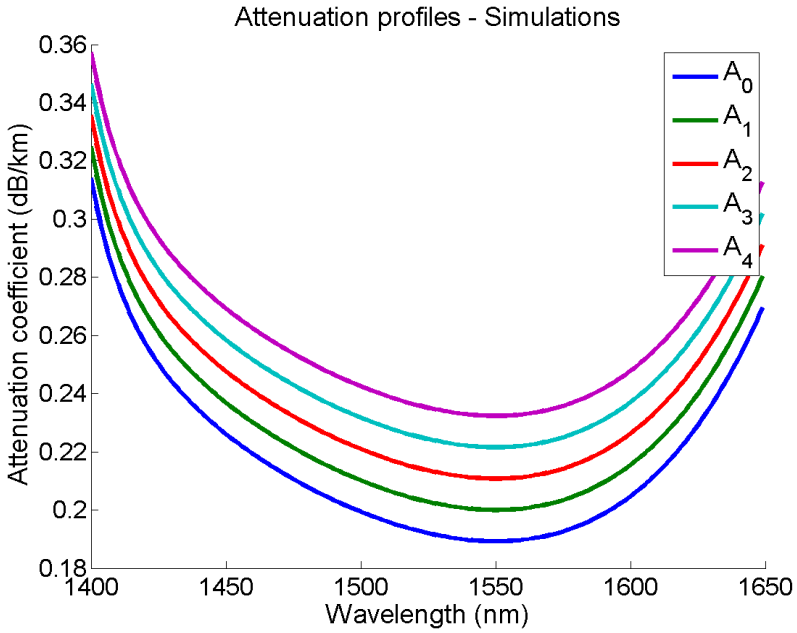

Figure 5.1: Attenuation profiles studied.

5.3 Results

This section reports the simulation results obtained in terms of AGC accuracy in relation to the total power (all 40 channels) and in relation to the channels power (channels taken separately). The impact of this calibration procedure on the amplifiers gain flatness and noise figure is also presented.

5.3.1 AGC accuracy in relation to the total power

Figure 5.2(a) shows the DRA performance in terms of AGC accuracy for the total power of the amplifier with the A_0 profile. This amplifier power masks and the Max, $Mean$ and Min values were already defined in Section 2.2.2.

Figures 5.2(b), (c), (d) and (e) show the AGC error of the amplifier in relation to the total power for all the A_F profiles, $F \in \{1, .., 4\}$, before and after applying the calibration procedure at different P_{off} [29]. In these figures, the results are presented regarding the $Mean$ and Max values. The continuous lines with the filled symbols show the AGC error before applying the calibration (BC) and the dotted lines with empty symbols show the AGC error after the calibration (AC). With the A_1 profile, for almost all the P_{off} power values in which the DRA calibration is applied, the AGC error decreases (by observing the decrease of the $Mean$ value). At $P_{off} = 0$ dBm, the AGC error increases. This degradation occurs due to the approximation done by using Hypothesis 1 and by adding an offset to the polynomials calculation, that cause higher AGC errors than

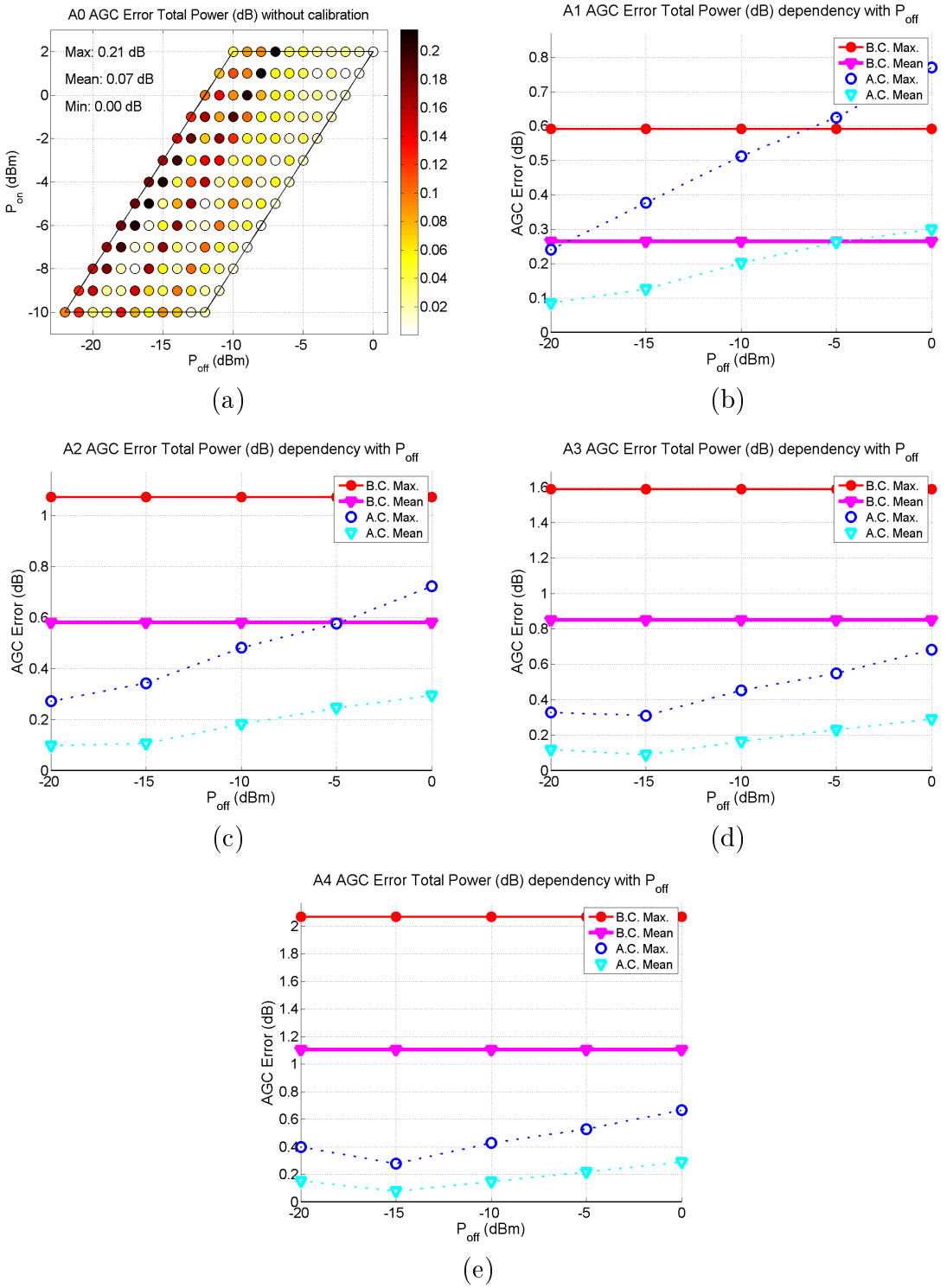

Figure 5.2: Simulation results in relation to the total power: (a) characterization of the amplifier with the A_0 profile; (b) calibration AGC accuracy performance with the A_1 profile; (c) calibration AGC accuracy performance with the A_2 profile; (d) calibration AGC accuracy performance with the A_3 profile; (e) calibration AGC accuracy performance with the A_4 profile.

without applying the calibration procedure. More generally, if the attenuation profile of the in-field transmission fiber is very close to the attenuation profile of the fiber used in the laboratory for the GCPs generation, the AGC accuracy improvement after the DRA calibration is almost imperceptible. On the other hand, if the attenuation profile shows some distance from the laboratory profile (A_0), as seen in profiles A_F, $F \in \{2, 3, 4\}$, then the calibration procedure notably improves the AGC accuracy of the DRA.

More detailed results obtained with the A_4 profile are presented in Appendix B.

5.3.2 AGC accuracy in relation to the channels power

The AGC accuracy study in relation to the channels power, showed in Figure 5.3, is only done for the following cases:

- With the A_0 profile, which is the best case since the GCPs were generated with this fiber profile;
- With the A_4 profile, which is the more extreme case, where the fiber attenuation increased a lot in relation to the initial A_0 profile.

Figure 5.3(a) (Figure 5.3(b)) shows the DRA performance in terms of the mean (maximum) of the AGC errors of all the channels with the A_0 profile. Figure 5.3(c) (Figure 5.3(d)) show the AGC error of the amplifier in relation to the mean (maximum) of the AGC errors of all the channels with the A_4 profile before and after applying the calibration procedure at different P_{off}. In all cases, the AGC accuracy improved after the DRA calibration. However, the AGC errors before and after the calibration procedure remain very high in relation to the total power analysis realized in the previous section. This is due to the ripple of the amplifier. Figure 5.3(e) shows the AGC errors of all the channels at point P, which is the operation point at the maximum P_{off} when operating with the maximum target gain $TG = 12\ dB$ (defined in Figure 5.3(a)). It is remarkable that, even if most of the channels AGC accuracy improved after applying the calibration procedure, some channels were not corrected and got higher AGC errors. This behavior can be explained by looking at Figure 5.3(f) that represents the channels gains at point P. Before calibration, the channels near the 195 THz frequency are already close to their 12 dB target gain. Therefore, when applying the calibration procedure to correct all the other channels, the pump power increases and the channels near the 195 THz frequency overpass the 12 dB target gain, leading to higher AGC errors. Without any ripple of the amplifier, all the channels would be corrected appropriately. The ripple is a physical limitation that depends on the pump lasers wavelength and power combinations [4]. As a conclusion, it is possible to say that the calibration procedure aims to correct the channels group behavior even if it has to degrades some isolated channels.

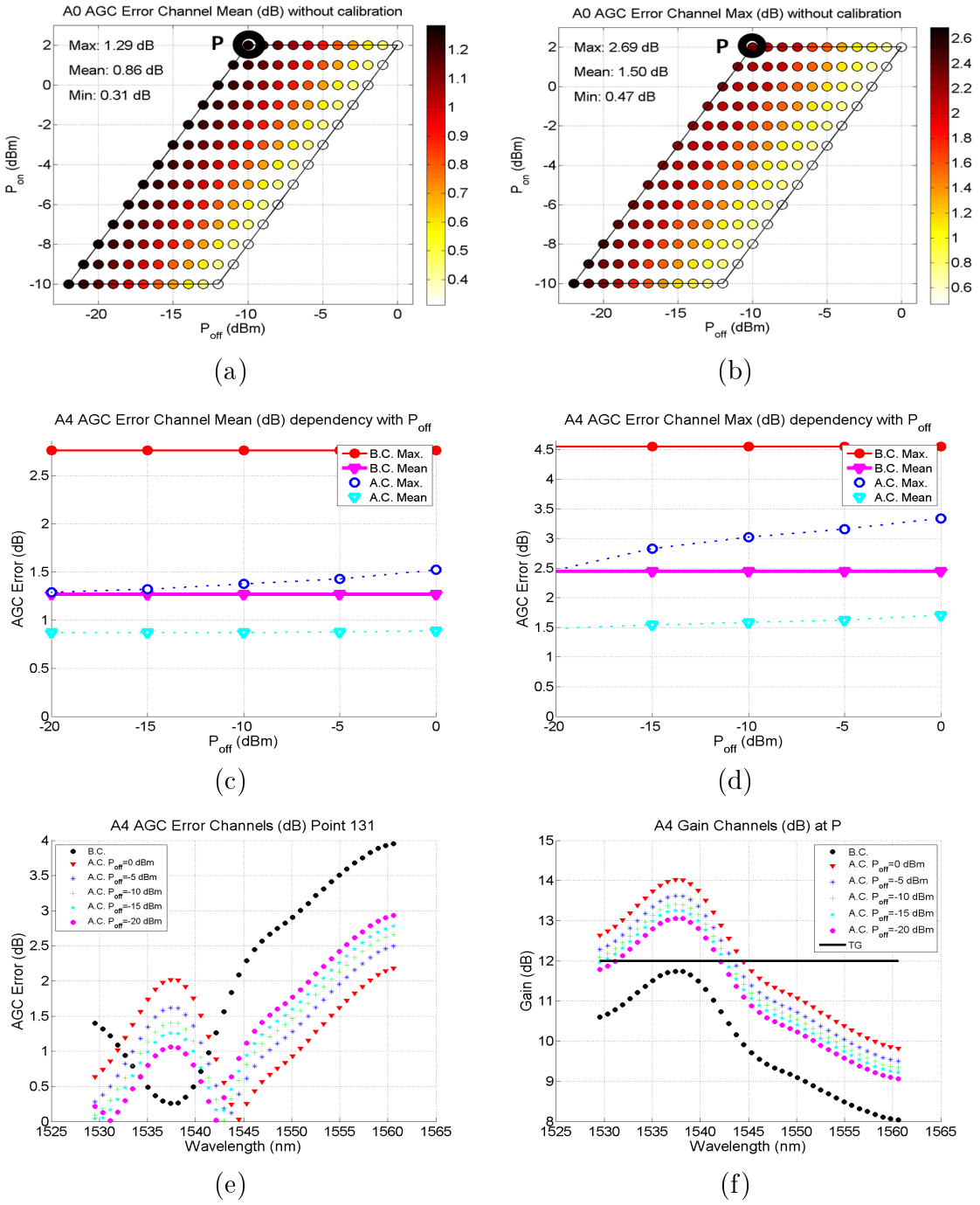

Figure 5.3: Simulation results in relation to the channel power: (a) characterization of the amplifier with the A_0 profile, mean of the channels AGC errors; (b) calibration AGC accuracy performance with the A_1 profile, maximum of the channels AGC errors; (c) calibration AGC accuracy performance with the A_4 profile, mean of the channels AGC errors; (d) calibration AGC accuracy performance with the A_4 profile, maximum of the channels AGC errors; (e) calibration AGC accuracy performance with the A_4 profile at point P for all the channels; (f) calibration gain correction performance with the A_4 profile at point P for all the channels.

More detailed results obtained with the A_4 profile are presented in Appendix B.

5.3.3 Gain flatness

The gain flatness study, showed in Figure 5.4, is only done for the following cases:

- With the A_0 profile, which is the best case since the GCPs were generated with this fiber profile;
- With the A_4 profile, which is the more extreme case since the fiber attenuation increased a lot in relation to the initial A_0 profile.

Figure 5.4(a) shows the ripple of the DRA with the A_0 profile. Figure 5.4(b) shows the ripple of the amplifier with the A_4 profile before and after applying the calibration procedure at different P_{off}. The ripple of the amplifier increases after calibration because the calibration process leads to an increase of the pump power since the A_4 profile has higher attenuations than the A_0 profile. This pump power increase causes a higher gain gap between channels which explains the higher ripple measured.

More detailed results obtained with the A_4 profile are presented in Appendix B.

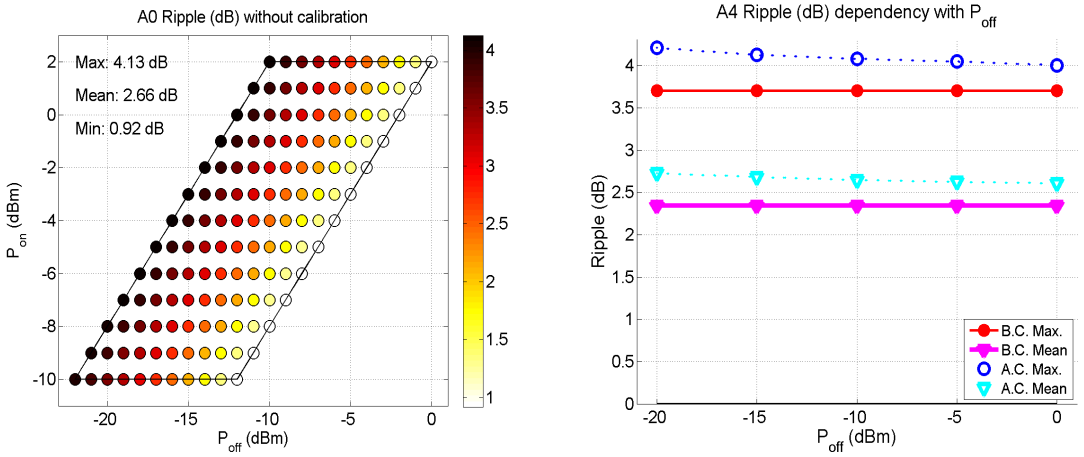

(a) (b)

Figure 5.4: Simulation results in relation to the gain flatness: (a) characterization of the amplifier with the A_0 profile, ripple; (b) gain flatness performance before and after calibration at various P_{off} with the A_4 profile.

5.3.4 Noise Figure

The noise figure study, showed in Figure 5.5, is only done for the following cases:

- With the A_0 profile, which is the best case since the GCPs were generated with this fiber profile;
- With the A_4 profile, which is the more extreme case since the fiber attenuation increased a lot in relation to the initial A_0 profile.

Figure 5.5(a) shows the noise figure of the DRA with the A_0 profile. Figure 5.5(b) shows the noise figure of the amplifier with the A_4 profile before and after applying the calibration procedure at different P_{off}. The calibration procedure almost doesn't have an impact on the noise noise figure. More detailed results obtained with the A_4 profile are presented in Appendix B.

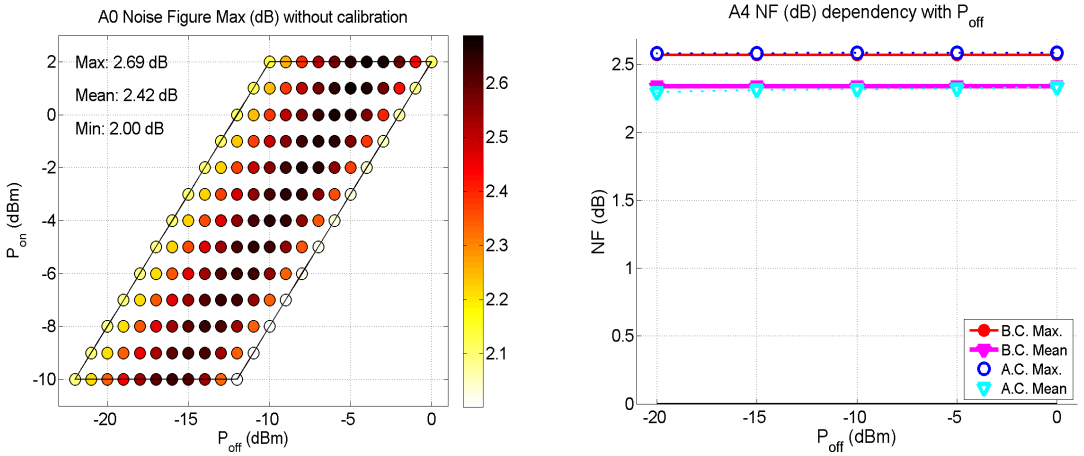

(a) (b)

Figure 5.5: Simulation results in relation to the noise figure: (a) characterization of the amplifier with the A_0 profile, noise figure; (b) noise figure performance before and after calibration at various P_{off} with the A_4 profile.

Chapter 6

Experimental results

6.1 Experimental setup and configurations studied

All the experiments were realized at CPqD Foundation. The experimental setup for the validation of the proposed DRA calibration procedure is almost identical to the simulation setup introduced in Section 5.1. The only difference is in the transmission fiber properties. Indeed, the experimental validation is done for transmission fibers of different attenuation profiles and with splices located at several distances from the DRA pump lasers, as presented in Figure 6.1. Three main configurations are studied:

- Configuration A: the transmission fiber is composed of two SMF spans separated with a splice situated at 4.5 km from the amplifier pump lasers (Figure 6.1(a)). The splice attenuations chosen are 0 dB, 1 dB, 2.1 dB and 3.2 dB.
- Configuration B: the transmission fiber is composed of two SMF spans that suffered fiber aging (higher attenuation than conventional SMFs) separated by a splice situated at 10.06 km from the amplifier pump lasers (Figure 6.1(b)). The splice attenuations chosen are 0 dB, 0.9 dB, 2.1 dB and 3.3 dB.
- Configuration C: the transmission fiber is composed of a low loss (lower attenuation than conventional SMFs) SMF span (Figure 6.1(c)).

The pump power provides amplification to the signal only for a few kilometers near the pump lasers (a dozen typically). This distance vary with the fiber attenuation profile, the chemical composition of the fiber, the presence of splices or connectors and fiber stresses. Modifying the properties of this fiber stretch has an influence on the pump power efficiency for the Raman amplification and thus on the Raman gain and AGC accuracy. The experiments realized are pertinent to validate the proposed DRAs

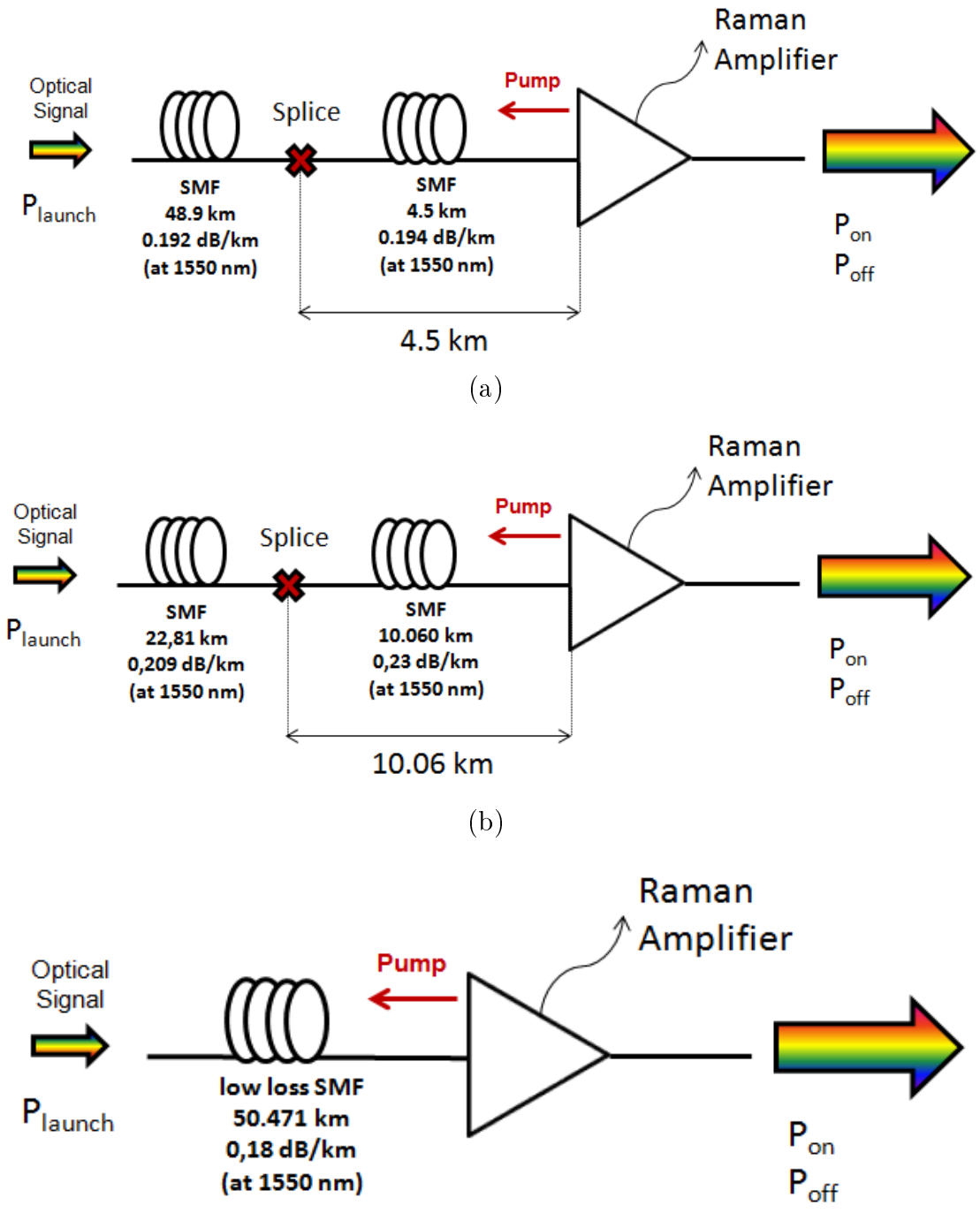

Figure 6.1: Experimental configurations with fibers of different attenuation profiles and with splices located at several distances from the DRA pump lasers: (a) configuration A; (b) configuration B; (c) configuration C.

calibration procedure since the properties of the fiber are modified in many ways near the pump lasers.

6.2 Splice realization setup

Figure 6.2 shows how splices of different attenuations are realized between SMFs. A fixed power laser at 1550 nm wavelength is used at the input of the first SMF span. A power meter is used at the ouput of the second SFM span to measure the total output power. The realization of a 3 dB splice attenuation, for example, take the following steps:

1. A 0 dB splice is created between the SMFs with the fusion splicer. In fact, a perfect splice has an attenuation of about 0.01 dB. This attenuation is negligible in relation to the final splice attenuation desired;
2. The output power (P^1_{out}) is measured with the power meter;
3. The fiber splice is broken;
4. A variable attenuation splice is realized with the fusion splicer. To do so, the fusion splicer dislocates the SMF alignment from the ideal at the splice spot. When the output power measured at the power meter is $P^2_{out} = P^1_{out} - 3$ dB, the 3 dB splice is realized.

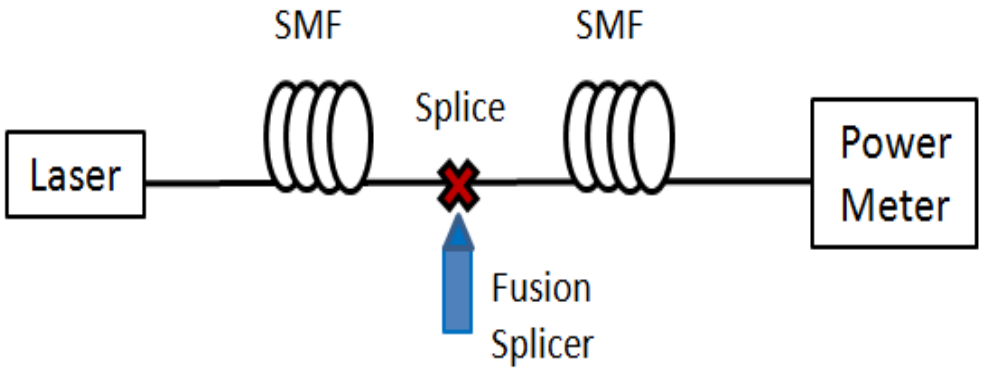

Figure 6.2: Splice setup.

6.3 Experimental GCPs generation

The experimental GCPs are generated in the configuration A (see Figure 6.1(a)) with a splice of 0 dB loss according to the following two stages:

- First stage: The total launch power P_{launch} is varied in 66 steps with a granularity of 0.5 dB in order to vary $P_{\text{off}} = P_{\text{launch}} - Loss$ from 0 to -32.5 dBm.
- Second stage : Executed for each step of the first stage and consists in varying the pump power of the amplifier in 100 steps with an exponential (base 10) granularity between the minimum pump power (10 mW) and the maximum pump power (360 mW).

Then, the original characterization of the amplifier in terms of AGC accuracy, based on the GCPs previously generated and in the configuration A (see Figure 6.1(a)) with a splice of 0 dB loss, is performed. The referring amplifier power mask is presented in Figure 6.4(b) and constitutes the base for all the interpretations of the experimental results reported in the next section.

6.4 Pump power limitations

As mentioned in Section 5.1, the nominal power of the lasers is 360 mW. When processing the calibration procedure in cases where the transmission fiber has higher attenuations than the fiber used to generate the GCPs, the pump power increases. At a given operation point of the DRA, if the pump power calculated for AGC accuracy is above this nominal power, the lasers will deliver their maximum power, that is the nominal power. Figure 6.3 shows the post-calibration calculated pump power for configuration B with a 0.9 dB attenuation splice. It should be noticed that the pump power already overpassed the lasers nominal power at $TG = 6\ dB$. For higher target gains, the DRA will never be able to provide enough pump power for the amplification and there will be AGC errors. These AGC errors are not due to any lack of precision of the calibration procedure but to a physical limitation. If the nominal power of the pump lasers would be higher, there wouldn't be this limitation and the calibration procedure would be efficient. Therefore, the experimental results that are presented in the next section only consider AGC accuracy performance evaluations of the calibration procedure for target gains that do not suffer this power limitation.

6.5 Results

The experiments are realized only in relation to the total power (all 40 channels). The experimental results are presented regarding the Min, $Mean$ and Max values, with and without calibration at different P_{off} in Figure 6.4 in relation to the configuration A, in Figure 6.5 in relation to the configuration B and in Figure 6.6 in relation to

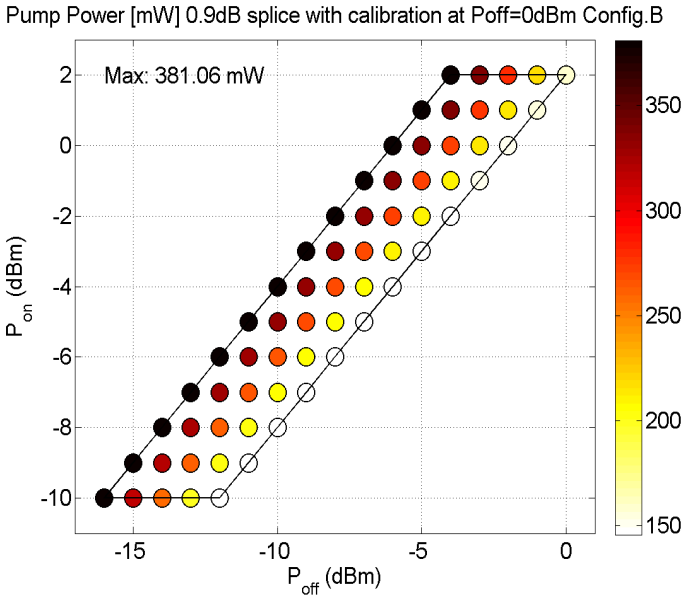

Figure 6.3: Post-calibration calculated pump power for configuration B with a 0.9 dB attenuation splice.

the configuration C. The continuous lines with the filled symbols show the AGC error before applying the calibration (BC) and the dotted lines with empty symbols show the AGC error after the calibration (AC). For all the cases, the calibration procedure notably improves the AGC accuracy. For some cases, like in Figure 6.5(c) at $P_{off} = -10$ dBm for example, the calibration procedure is so effective that the AGC errors are even lower than for the original characterization of the amplifier in the situation where the GCPs were generated (Figure 6.4(b)), which should have been the best result achievable. In these particular cases, the calibration procedure may have corrected a pump power control approximation in the amplifier firmware (where the polynomials are substituted by a neural network for time calculation efficiency) or an alteration in the connectors properties between the GCPs generation and the original characterization. Also, it is important to notice that the calibration procedure is not only efficient for transmission fibers that have higher attenuation profiles and addition of splices (like in Figures 6.4 and 6.5), but also for transmission fibers of lower attenuation profiles in relation to the original fiber (Figure 6.6).

More detailed results obtained from configuration A with a 3.2 dB attenuation splice, configuration B with a 0.9 dB attenuation splice and configuration C are presented in Appendix C.

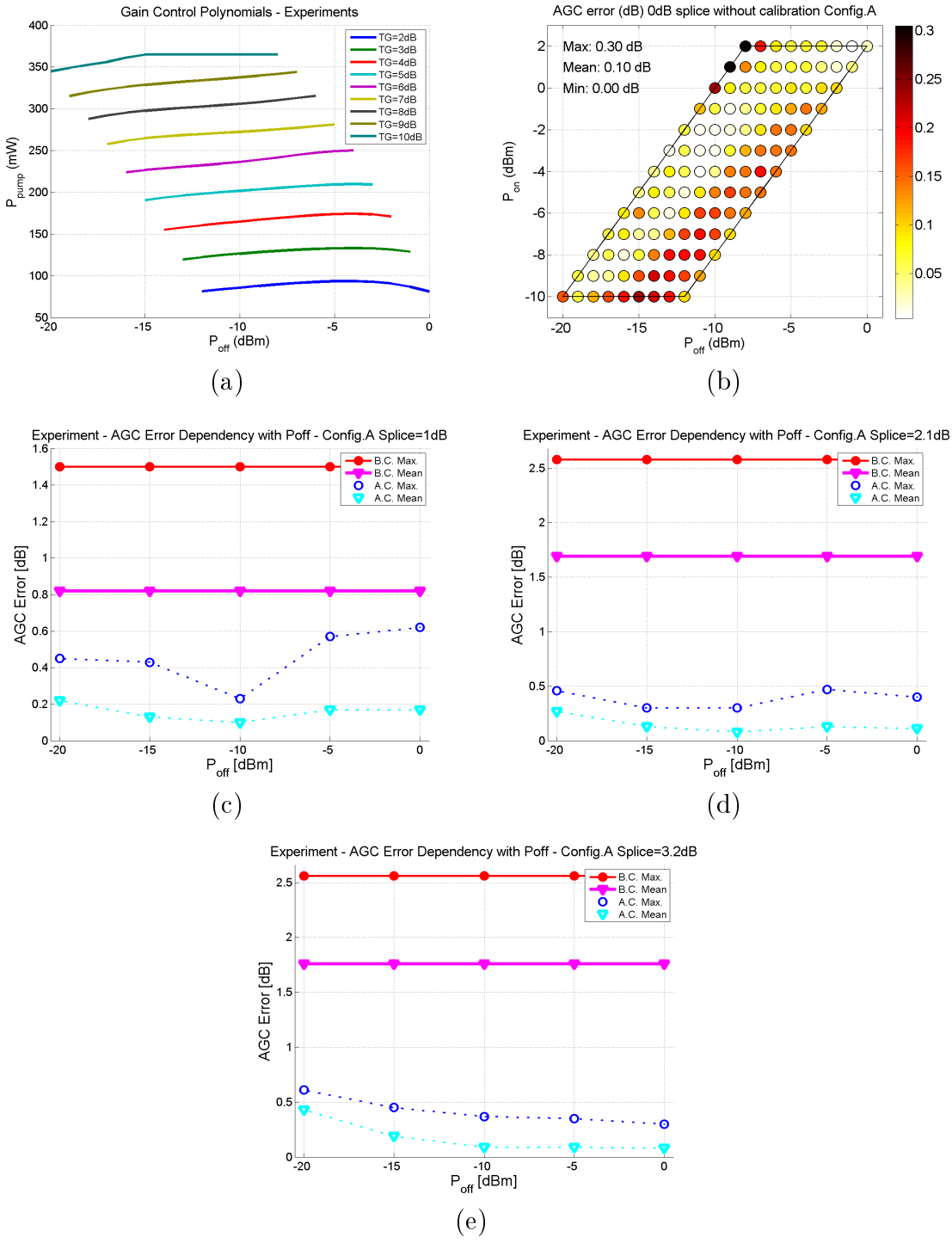

Figure 6.4: Experimental GCPs and experimental results in the configuration A: (a) gain control polynomials generated, experiments; (b) characterization of the amplifier in the configuration A, with a 0 dB splice; (c) calibration AGC accuracy performance in the configuration A, with a 1 dB splice; (d) calibration AGC accuracy performance in the configuration A, with a 2.1 dB splice; (e) calibration AGC accuracy performance in the configuration A, with a 3.2 dB splice.

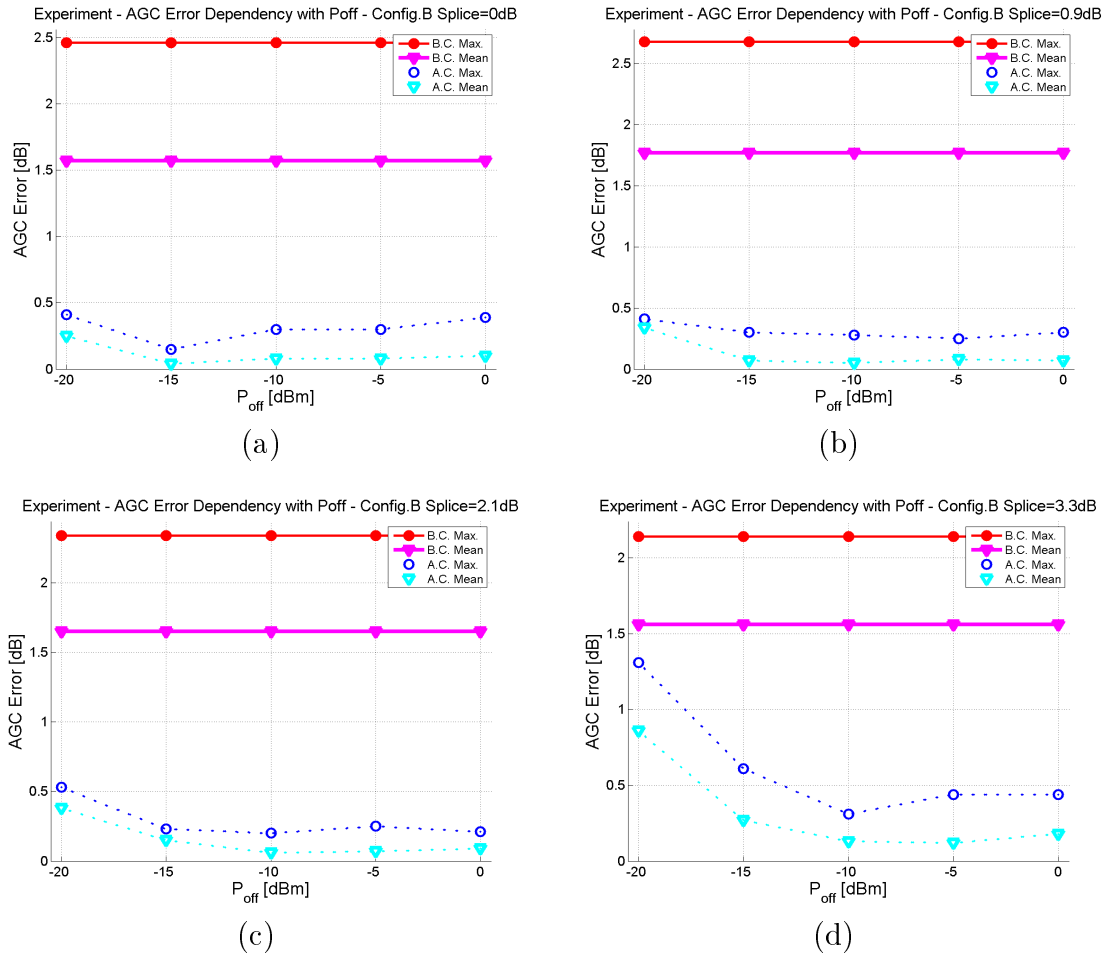

Figure 6.5: Experimental results in the configuration B: (a) calibration AGC accuracy performance in the configuration B, with a 0 dB splice; (b) calibration AGC accuracy performance in the configuration B, with a 0.9 dB splice; (c) calibration AGC accuracy performance in the configuration B, with a 2.1 dB splice; (d) calibration AGC accuracy performance in the configuration B, with a 3.3 dB splice.

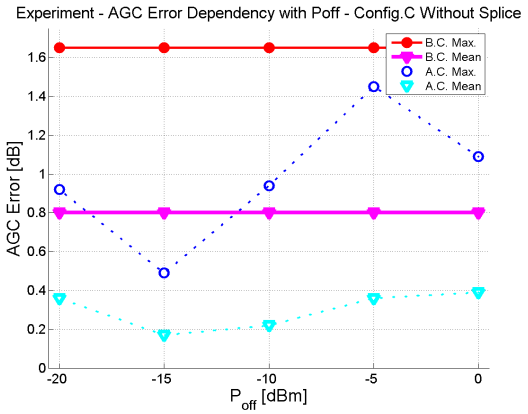

Figure 6.6: Experimental results in the configuration C.

Chapter 7

Conclusion

This Masters dissertation proposes a new in-field calibration procedure of the DRA to operate in AGC mode with accuracy. To be implemented, the proposed calibration procedure does not require any information about the in-field fiber characteristics or about the launched signal power. Furthermore, the calibration procedure can be implemented only with the traditional components that compose the DRA so there is no increase in production cost.

The performance of the calibration procedure was proved in simulations with transmission fibers of different attenuation profiles. Initially, pump power adjustments were performed with the lower attenuation profile. Then, higher attenuation profiles were used in order to see the AGC accuracy degradation that could occur in field installations due to fiber aging, for example. Finally, the calibration procedure was performed to evaluate its efficiency in correcting the AGC errors. In the more extreme case, that is with the higher attenuation profile, the mean of the AGC errors for all the operation points of the amplifier dropped from 1.1 dB before calibration to below 0.4 dB after calibration.

Still in simulations, the impact of the calibration procedure on the gain flatness was studied. With the fibers of higher attenuation than the one of the initial fiber, the calibration procedure corrected the AGC errors by increasing the pump power. As a consequence, the channels power gap increased and engendered a worse gain flatness. However, compared to the AGC accuracy enhancements obtained with calibration, the gain flatness degradation was insignificant.

Other simulations showed that the calibration procedure almost didn't have an impact on the noise figure.

Finally, the calibration procedure efficiency was validated experimentally with fibers of different attenuation profiles and with splices located at several distances from

the DRA pump lasers. By adding slices in the optical link it was possible to prove that the calibration procedure was efficient not only with additional distributed attenuations, like in the simulation case, but also with punctual attenuations (e.g., fiber splices, connectors, fiber bends). Various configurations were studied and in the more extreme case, that is configuration A where two SMF spans were separated by a splice of 3.2 dB attenuation situated at 4.5 km from the pump lasers, the mean of the AGC errors for all the operation points of the amplifier dropped from 1.75 dB before calibration to below 0.5 dB after calibration.

Future Work: The proposed calibration procedure requires to turn off the pump lasers for a few seconds to measure P_{off}. At the field installation of the DRA or after repairing a fiber break with a splice the pump lasers are already turned off, so there is no problem. However, if the calibration procedure is processed when the amplifier is operating, these pump power variations cause signal power variations and network perturbations. To avoid such a scenario, it would be interesting to develop a pump power adjustment that can be processed with optical traffic. A possible solution would be to use an OTDR along with the DRA to evaluate at any time the transmission fiber attenuations and correct the pump power. However, this technique alone cannot solve everything. Indeed, the OTDR cannot measure the Raman gain coefficient of the in-field fiber. Also, the OTDR is blind to all measurements near its laser due to the pulse width. Finally, a relation between the fiber attenuation at the OTDR pulse wavelength and at the DRA pump lasers wavelengths needs to be found.

Another interesting study would be to evaluate the calibration procedure efficiency modifying the number of pump lasers, their wavelength and the way to control their power.

Bibliography

[1] C. V. N. Index, "Global mobile data traffic forecast update, 2014-2019," *White Paper, February*, 2015.

[2] O. Gerstel, M. Jinno, A. Lord, and S. B. Yoo, "Elastic optical networking: A new dawn for the optical layer?" *Communications Magazine, IEEE*, vol. 50, no. 2, pp. s12–s20, 2012.

[3] G. P. Agrawal, *Fiber-optic communication systems*. John Wiley & Sons, 2012, vol. 222.

[4] F. M. Mustafa, A. A. Khalaf, and F. Elgeldawy, "Multi-pumped Raman amplifier for long-haul UW-WDM optical communication systems: Gain flatness and bandwidth enhancements," in *Advanced Communication Technology (ICACT), 2013 15th International Conference on*. IEEE, 2013, pp. 122–127.

[5] C. Headley and G. P. Agrawal, *Raman Amplification In Fiber Optical Communication Systems*. San Diego, CA, USA: Academic Press, 2005.

[6] Finisar, "Operational issues in the deployment of Raman amplifiers," *White Paper, November*, 2012.

[7] B. Clouet, "Method and arrangement for in service Raman gain measurement and monitoring," US patent Application, original assignee: Nokia Siemens Networks Oy, application number: US 13/392,654, date of filing: 08/25/2009, publication number: US 20120177366 A1, date of publication: 07/12/2012.

[8] U. Ghera, A. Shlifer, D. Berger, M. Zaacks, and D. Menashe, "Automatic measurement and gain control of distributed Raman amplifiers," US patent Application, original assignee: Red-C Optical Networks Ltd., application number: US 12/946,899, date of filing: 11/16/2010, publication number: US 20110141552 A1, date of publication: 06/16/2011.

[9] D. Atlas, M. Taleghani, M. Mahbobzadeh, and K. Hamilton, "Method for controlling signal gain of a Raman amplifier," US patent, original assignee: Adva Optical Networking Se, application number: US 13/419,422, date of filing: 03/13/2012, publication number: US 8854726 B2, date of publication: 10/07/2014.

[10] U. Ghera, D. Meshulach, O. Eyal, and R. Klein, "Apparatus and method for a self-adjusting Raman amplifier," US patent, original assignee: Redc Optical Networks Ltd., application number: US 10/079,525, date of filing: 02/22/2002, publication number: US 6519082 B2, date of publication: 02/11/2003.

[11] D. Mongardien, "Method and an optical amplifier assembly for adjusting Raman gain," US patent application, original assignee: Alcatel, application number: US 11/583,018, date of filing: 10/19/2006, publication number: US 20070115537 A1, date of publication: 05/24/2007.

[12] C. Fu, P. Zhang, Y. Jiang, C. Yu, and C. Zhang, "Method of performing target raman gain locking and Raman fiber amplifier," US patent application, application number: US 13/323,455, publication number: US 20120327505 A1, date of publication: 12/27/2012.

[13] G. Charlet and C. Martinelli, "Gain monitor in a distributed Raman amplifier," European patent application, original assignee: Alcatel, application number: EP 20030292070, date of filing: 08/22/2003, publication number: EP 1508985 A1, date of publication: 02/23/2005.

[14] S. J. Kim, J. M. Kim, S. Y. Yoon, M. K. Choi, and W. B. Chae, "Self-automatic gain control distributed Raman fiber amplifier and automatic gain control method," US patent application, original assignee: Licomm Co., Ltd., application number: US 14/315,850, date of filing: 06/26/2014, publication number: US 20150002922 A1, date of publication: 01/01/2015.

[15] J. C. R. Oliveira, G. E. R. Paiva, J. R. F. Oliveira, and U. C. Moura, "Método de controle de ganho e dispositivo amplificador óptico híbrido para redes DWDM reconfiguráveis (in portuguese)," Brazilian patent application, original assignee: CPqD Foundation, application number: BR 10 2012 021156 4 A2 , date of filing: 08/23/2012, date of publication: 09/16/2014, international patent classification: H04B 10/2537.

[16] R. C. Alferness, "The evolution of configurable wavelength multiplexed optical networks. a historical perspective," *Proceedings of the IEEE*, vol. 100, no. 5, pp. 1023–1034, 2012.

[17] S. Kartalopoulos, *The Optical Waveguide: The Fiber*. Wiley-IEEE Press, 2009.

[18] S. Azodolmolky, M. Klinkowski, E. Marin, D. Careglio, J. S. Pareta, and I. Tomkos, "A survey on physical layer impairments aware routing and wavelength assignment algorithms in optical networks," *Computer Networks*, vol. 53, no. 7, pp. 926–944, 2009.

[19] S. Gringeri, B. Basch, V. Shukla, R. Egorov, and T. J. Xia, "Flexible architectures for optical transport nodes and networks," *Communications Magazine, IEEE*, vol. 48, no. 7, pp. 40–50, 2010.

[20] R. Ramaswami, K. Sivarajan, and G. Sasaki, *Optical networks: a practical perspective*. Morgan Kaufmann, 2009.

[21] S. J. Savory, "Digital coherent optical receivers: algorithms and subsystems," *Selected Topics in Quantum Electronics, IEEE Journal of*, vol. 16, no. 5, pp. 1164–1179, 2010.

[22] Cienas, "New "smart Raman" amplification provides Raman gain without the pain," http://www.ciena.com/connect/blog/Cienas-new-Smart-Raman-amplification-provides-Raman-gain-without-the-pain.html, accessed October 12, 2015.

[23] X. Feng, W. Zhang, X. Liu, and J. Peng, "A novel control method for on-off gain and gain tilt of fiber Raman amplifiers," *Chinese Optics Letters*, vol. 2, no. 4, pp. 196–199, 2004.

[24] R. B. Sargent, "Recent advances in thin film filters," in *Optical Fiber Communication Conference*. Optical Society of America, 2004, p. TuD6.

[25] J. R. Oliveira, J. C. Oliveira, and E. C. Ferreira, "Transient suppression of gain controlled EDFAs for optical reconfigurable optical networks applications," in *Frontiers in Optics*. Optical Society of America, 2008, p. FTuG3.

[26] Lumentum, "Wra-219 multichannel erbium-doped fiber amplifier (EDFA)," https://www.lumentum.com/sites/default/files/technical-library-items/wra219_ds_cms_tm_ae.pdf, accessed October 13, 2015.

[27] J. R. F. d. Oliveira, "Amplificador óptico híbrido Raman/EDFA com controle automático de ganho para redes DWDM reconfiguráveis (in portuguese)," Ph.D. dissertation, University of São Paulo, 2014.

[28] J. R. Oliveira, U. C. Moura, J. C. Oliveira, and M. A. Romero, "Hybrid distributed Raman/EDFA amplifier with hybrid automatic gain control for reconfigurable WDM optical networks," *Journal of Microwaves, Optoelectronics and Electromagnetic Applications*, vol. 12, no. 2, pp. 602–616, 2013.

[29] B. Sarti, M. Garrich, B. Roulle, I. Cassimiro, U. Moura, J. R. Oliveira, and M. H. Costa, "Field calibration procedure for enhanced automatic gain control of distributed Raman amplifiers," in *2015 SBMO/IEEE MTT-S International Microwave and Optoelectronics Conference*. Porto de Galinhas, Pernambuco, Brazil: IEEE, 2015.

Appendices

Appendix A

Noise figure for distributed Raman amplifiers

In this appendix, the superscripts linear and dB indicate that the variable are expressed "in linear" and dB respectively.

The noise figure (NF^{linear}) of an amplifier is the ratio of the SNR of the input signal to SNR of the output signal (both SNRs are obtained after measuring the optical power with a photodetector). It is a measure of how much the amplifier degrades the signal. In a distributed Raman amplified system, the equivalent noise figure, (NF_{eq}^{linear}), represents the noise figure an amplifier placed at the receiver end of the transmission span would need, in the absence of Raman amplification, to provide the same SNR as that obtained using distributed Raman amplification. The two equivalent systems are shown schematically in Figure A.1.

The loss in the span in Figure A.1(b) is $\alpha_s L$. Hence, the gain is $G^{linear} = (\alpha_s L)^{-1}$ and the noise figure of the unpumped span is $\alpha_s L$ (no noise added so $NF^{linear} = P_{in} / Pout$). A well-known expression for the noise figure for two cascaded amplifiers is given as $NF_{sys}^{linear} = NF1^{linear} + \left(NF2^{linear} - 1\right) / G1^{linear}$. Where $NF1^{linear}$ ($NF2^{linear}$) is the noise figure of the first (second) amplifier, and $G1^{linear}$ is the gain of the first amplifier. For the equivalent system in Figure A.1(b):

$$NF_{sys}^{linear} = NF_{eq}^{linear} \alpha_s L. \tag{A.1}$$

Equating the noise figure of the Raman amplified system to that of the equivalent system, it is seen that:

$$NF_{eq}^{linear} = \frac{NF_R^{linear}}{\alpha_s L} \quad or \quad NF_{eq}^{dB} = NF_R^{dB} - (\alpha_s L)^{dB} \tag{A.2a}$$

$$NF_R^{linear} = \frac{1}{G_N^{linear}} + \frac{P_{ASE}}{h\nu G_N^{linear}\Delta\nu} \tag{A.2b}$$

where G_N^{linear} is the linear gain of the DRA, P_{ASE} is the ASE noise power in W, $\Delta\nu$ is the optical bandwidth in Hz, ν is the channel frequency in Hz and h is the Plank constant in $J.s$.

From Eq. A.2 it is seen that NF_{eq}^{dB} can be less than zero. Such an amplifier is not physically realizable, but is indicative of the superior performance provided by the distributed Raman amplification, which cannot be matched by a discrete amplifier placed after the span. An intuitive if not rigorous explanation is that amplification always adds noise to the signal, degrading its SNR. In the best case, if the signal propagates along the fiber with no loss and with no amplification its SNR would be equal to its input value and the NF equal to one. The worst case is if the signal experiences the full loss of the span and then is amplified. This is the worst case because the gain required from the amplifier at the end of the span has increased; because more pump power is required, more amplified spontaneous emission (ASE) is generated in the amplifier. In addition the input signal power to the amplifier has decreased. The lower signal power means that the ASE can more successfully compete with the signal for gain in the amplifier. These two factors combine to lower the output SNR and increase the NF. If the transmission span is considered to be a series of discrete amplifiers, then the more evenly the gain is distributed along the fiber the less gain is required from each of the individual amplifiers and the higher the signal power into each of these amplifiers. This is why distributed amplification provides improved performance compared to discrete amplification. In addition it also explains why even when doing distributed Raman amplification, the more evenly gain is distributed along the fiber length the larger the improved performance provided by the distributed amplification scheme. In many of the discussions that follow the focus will be on raising the gain by more evenly distributing it along the fiber.

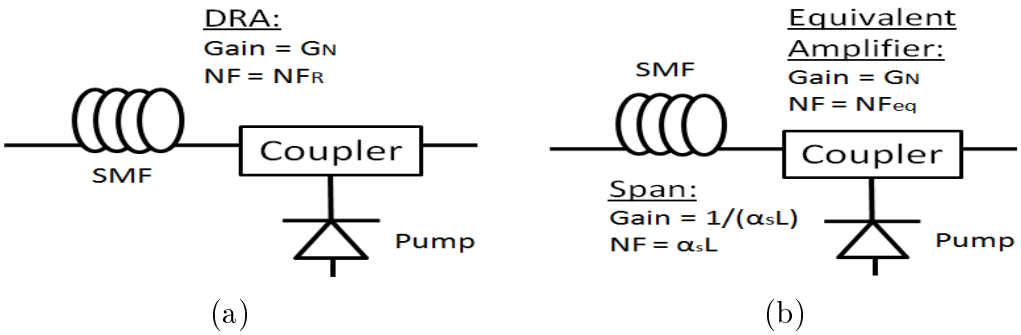

Figure A.1: Equivalent system for the NF measurement (source: Headley and Agrawal [5]): (a) schematic of a distributed Raman amplified system; (b) equivalent system of a transmission span and a discrete erbium-doped fiber amplifier.

Appendix B

Simulation results, a detailed study of the A_4 profile

This appendix presents detailed simulation results obtained with the A_4 profile which is the more extreme simulation case since the fiber attenuation increased a lot in relation to the initial A_0 profile (c.f., Figure 5.1). The results are reported before and after calibration at the extreme calibration P_{off} values ($P_{off} = 0\ dBm$ and $P_{off} = -20\ dBm$) in relation to:

- The AGC accuracy of the total power (all 40 channels) in Figure B.1;
- The AGC accuracy of the channels power (channels taken separately) in Figure B.2 and Figure B.3;
- The gain flatness in Figure B.4;
- The noise figure in Figure B.5.

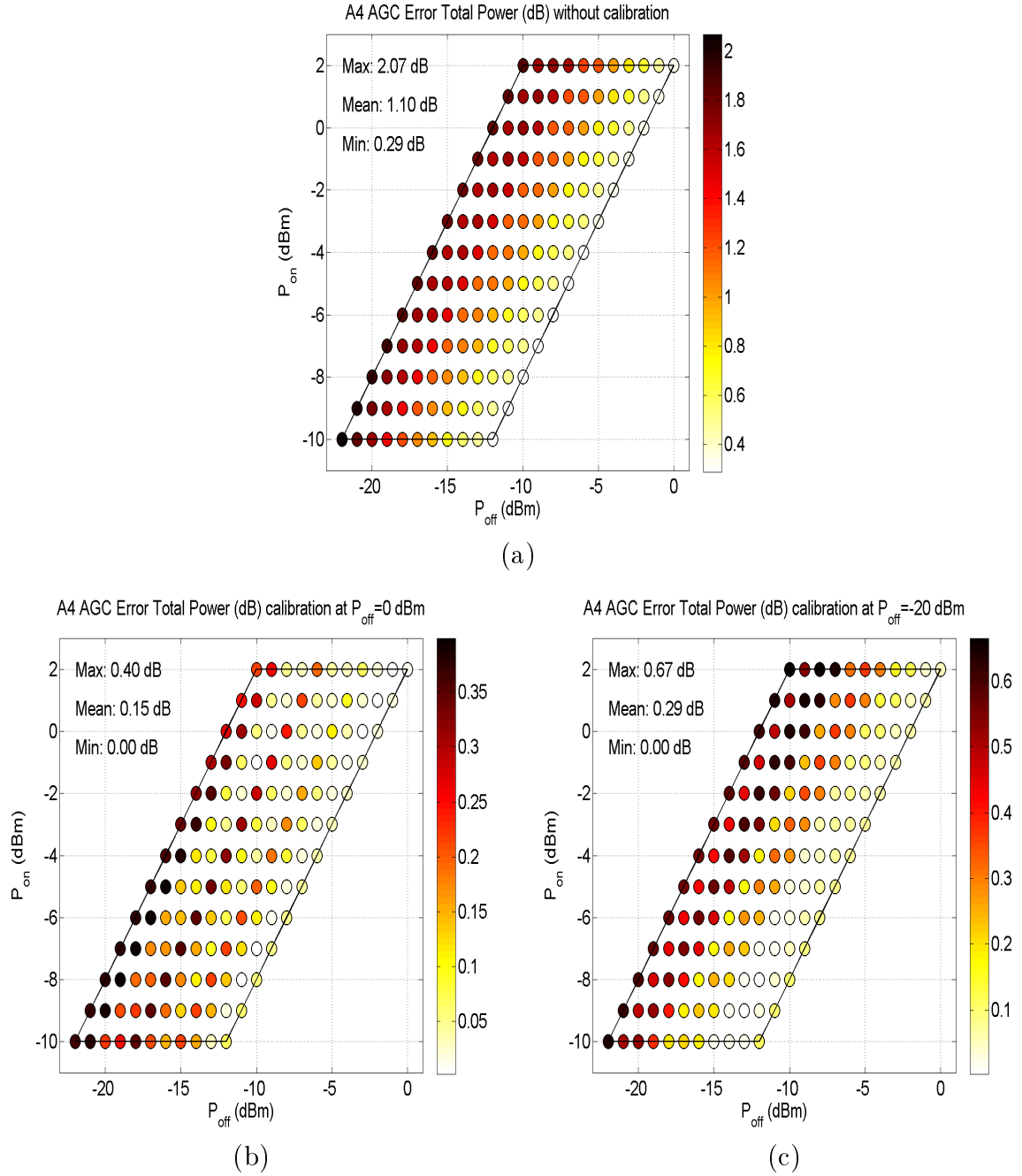

Figure B.1: Simulation results in relation to the total power, A_4 profile: (a) before calibration; (b) calibration at $P_{off} = 0$ dBm; (c) calibration at $P_{off} = -20$ dBm.

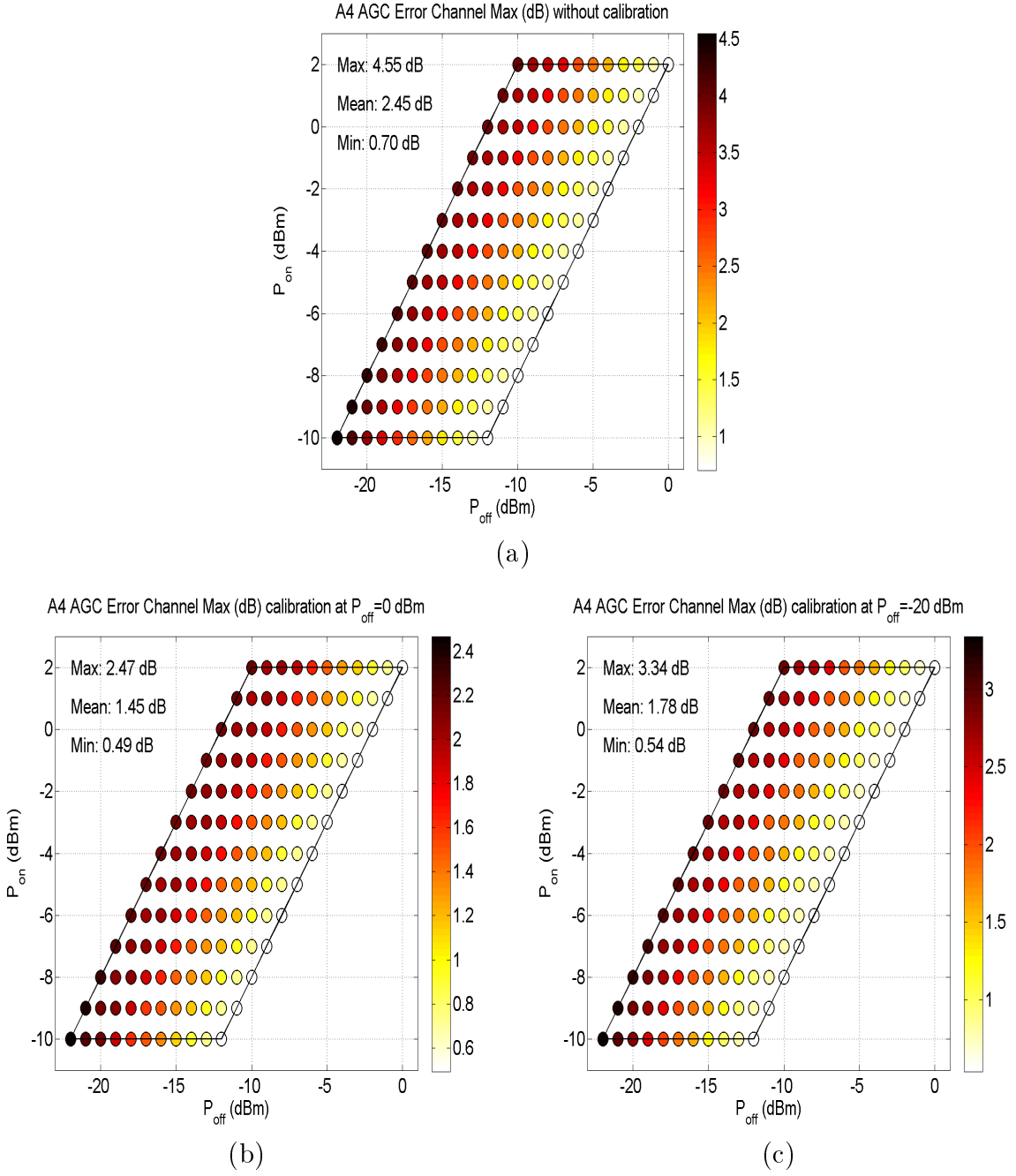

Figure B.2: Simulation results in relation to the channels power, maximum of the AGC errors of all the channels, A_4 profile: (a) before calibration; (b) calibration at $P_{off} = 0$ dBm; (c) calibration at $P_{off} = -20$ dBm.

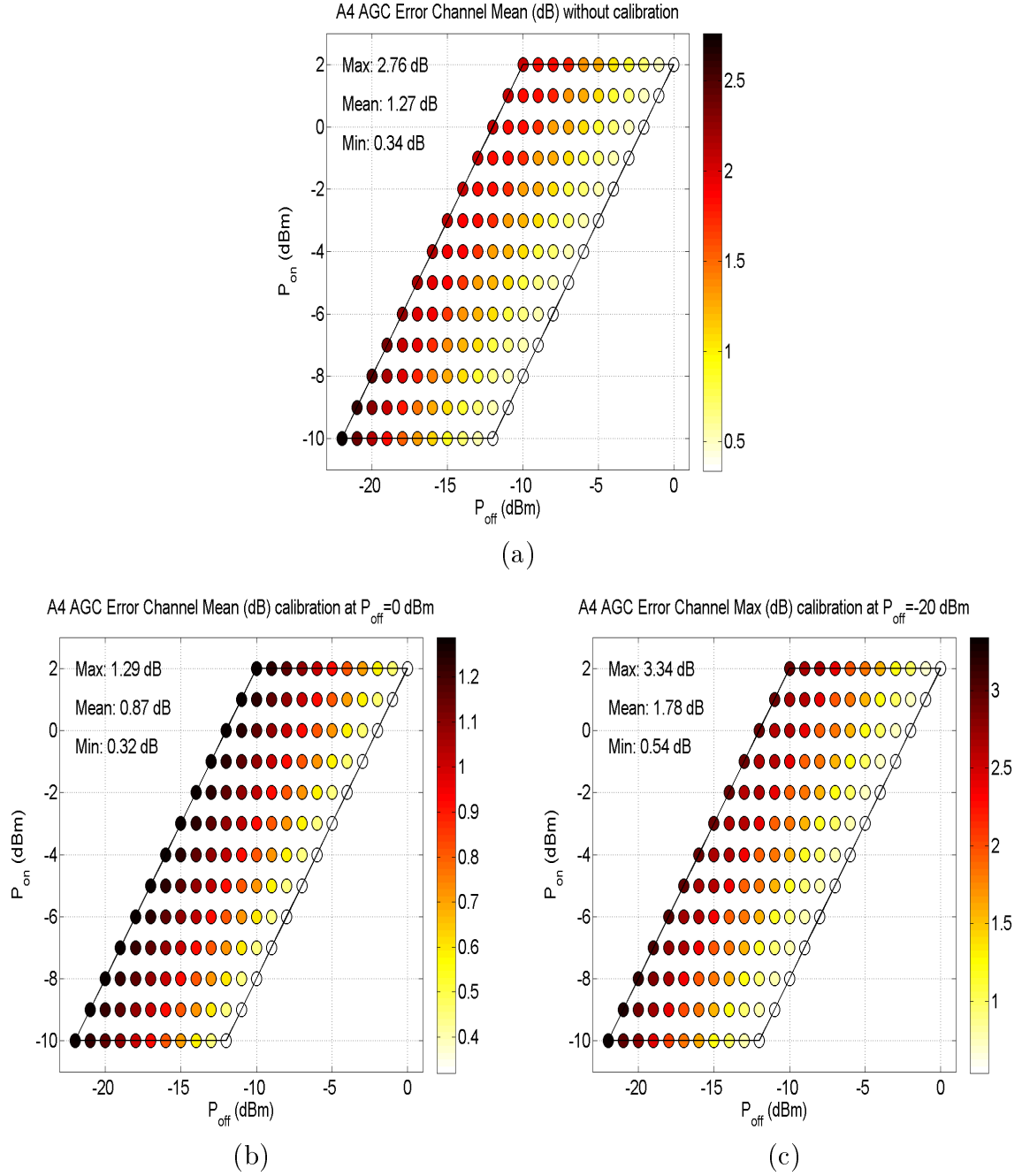

Figure B.3: Simulation results in relation to the channels power, mean of the AGC errors of all the channels, A_4 profile: (a) before calibration; (b) calibration at $P_{off} = 0$ dBm; (c) Calibration at $P_{off} = -20$ dBm.

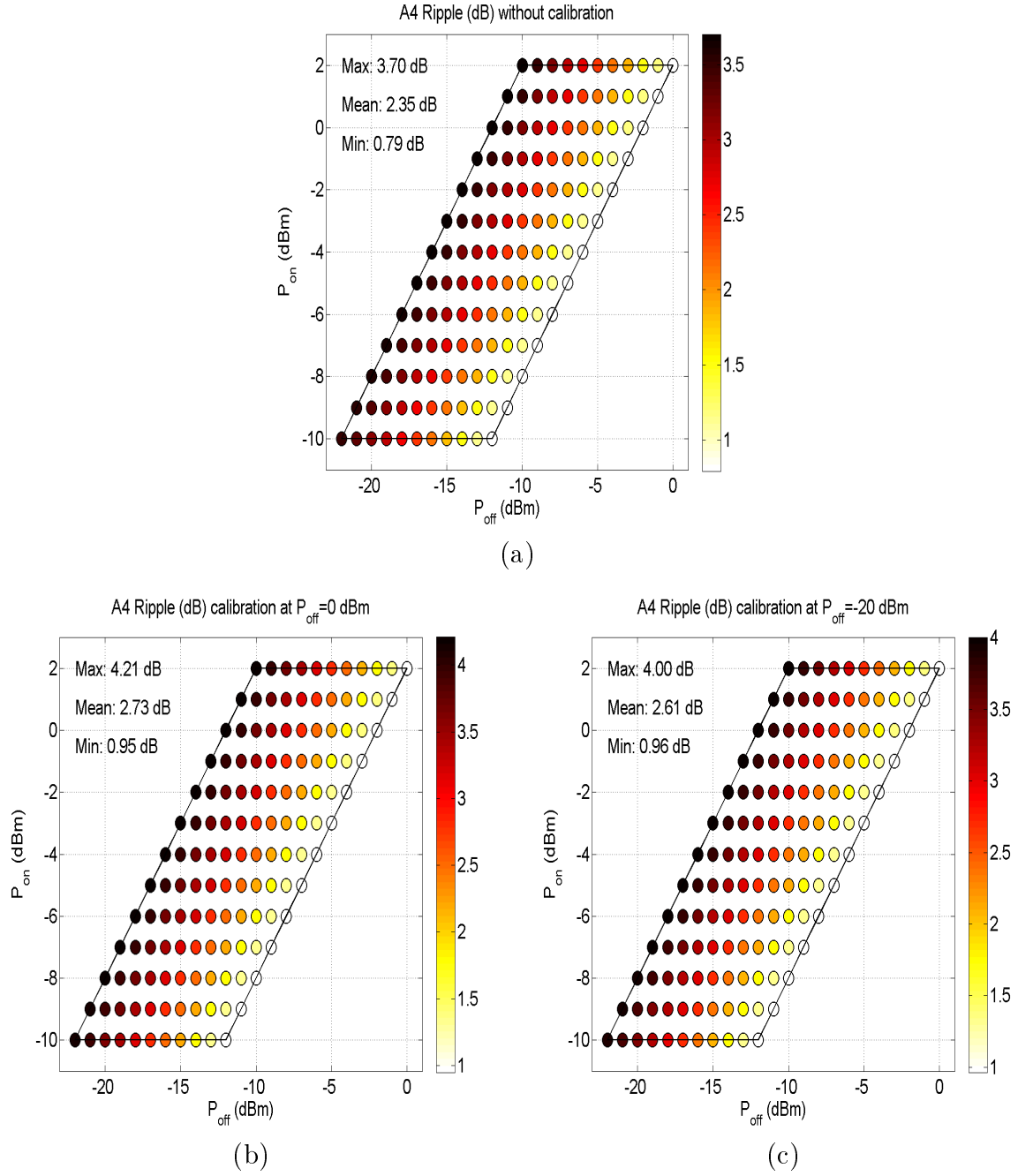

Figure B.4: Simulation results in relation to the gain flatness, A_4 profile: (a) before calibration; (b) calibration at $P_{off} = 0$ dBm; (c) calibration at $P_{off} = -20$ dBm.

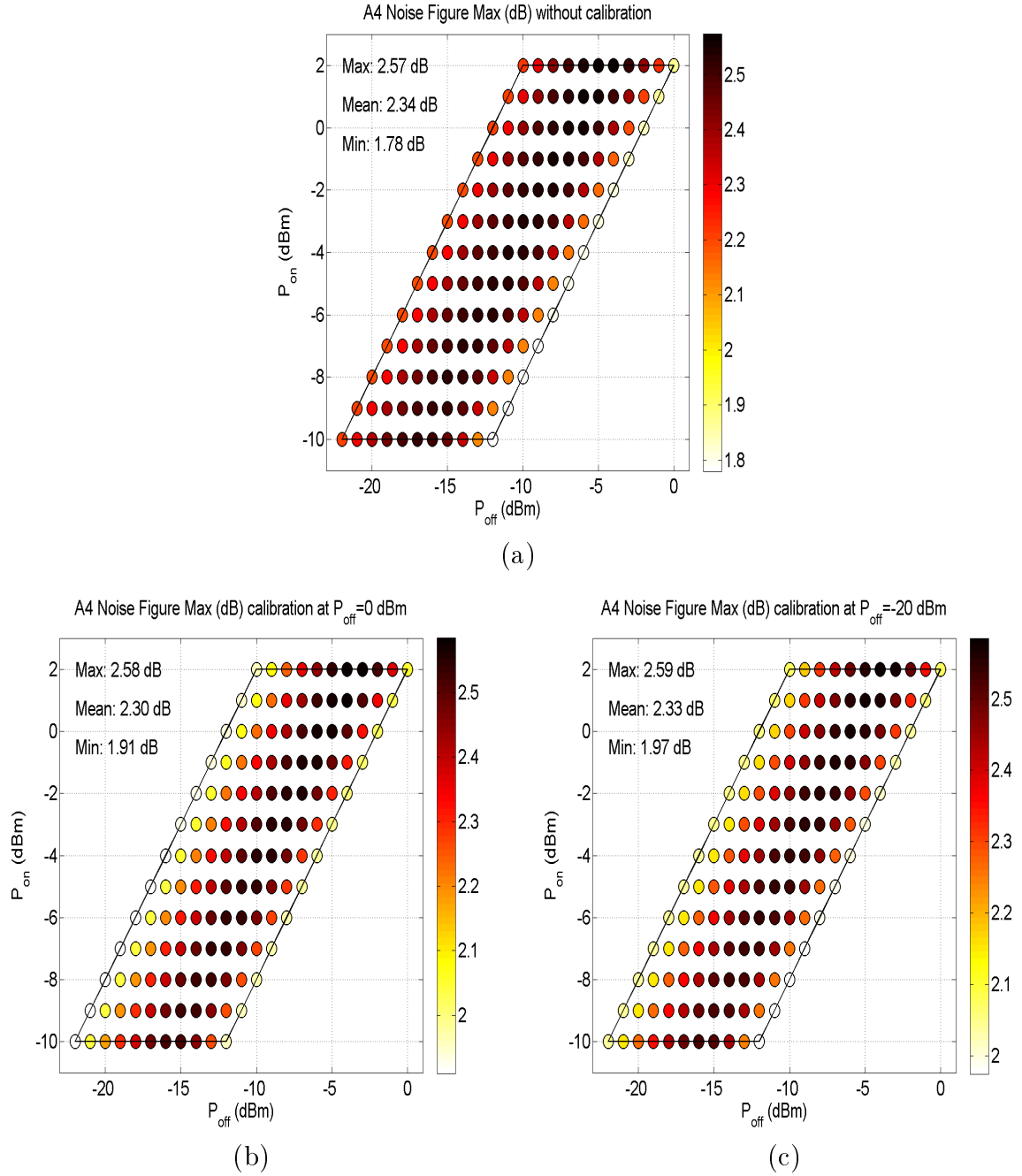

Figure B.5: Simulation results in relation to the noise figure, A_4 profile: (a) before calibration; (b) calibration at $P_{off} = 0$ dBm; (c) calibration at $P_{off} = -20$ dBm.

Appendix C

Experimental results, a detailed study for configurations A, B and C

This appendix presents detailed experimental results in relation to the total power obtained with:

- Configuration A with a 3.2 dB attenuation splice in Figure C.1;
- Configuration B with a 0.9 dB attenuation splice in Figure C.2;
- Configuration C in Figure C.3.

The results are reported before and after calibration at the extreme calibration P_{off} values ($P_{off} = 0\ dBm$ and $P_{off} = -20\ dBm$).

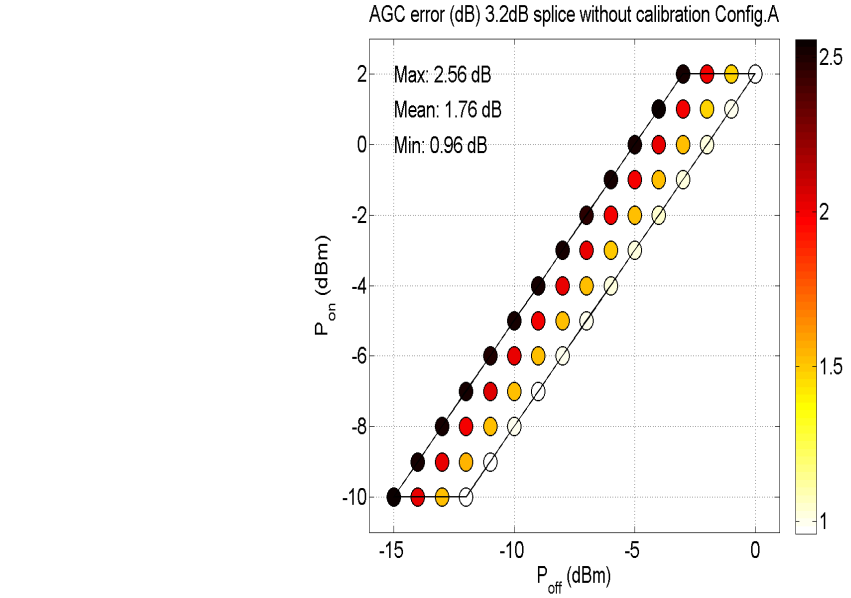

(a)

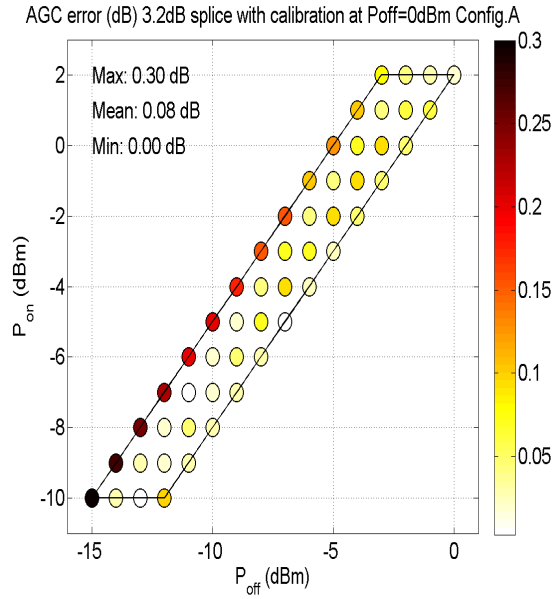

(b)

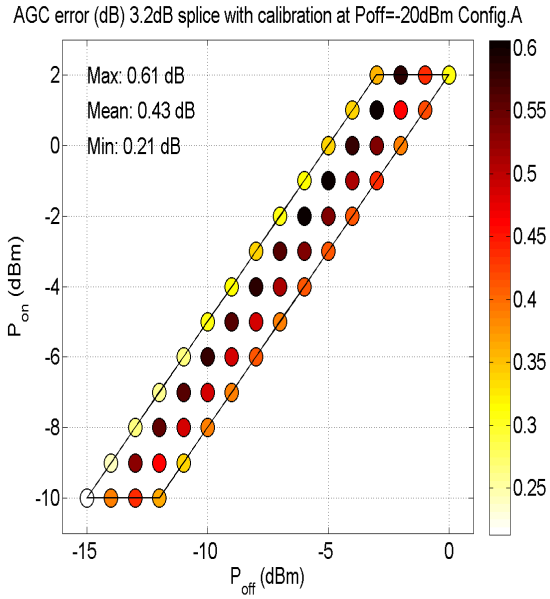

(c)

Figure C.1: Experimental results, configuration A with a 3.2 dB attenuation splice: (a) before calibration; (b) calibration at $P_{off} = 0$ dBm; (c) calibration at $P_{off} = -20$ dBm.

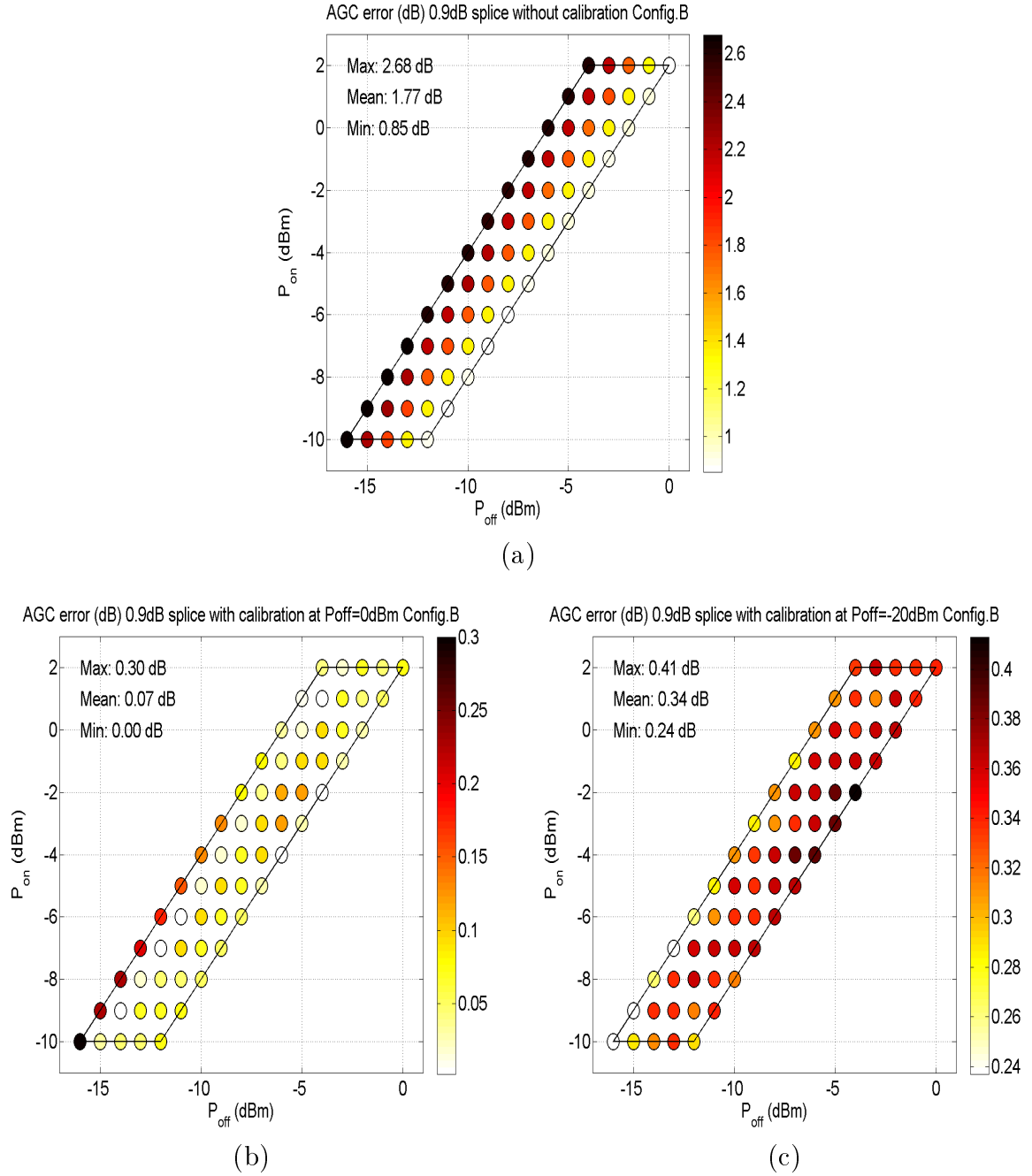

Figure C.2: Experimental results, configuration B with a 0.9 dB attenuation splice: (a) before calibration; (b) calibration at $P_{off} = 0$ dBm; (c) calibration at $P_{off} = -20$ dBm.

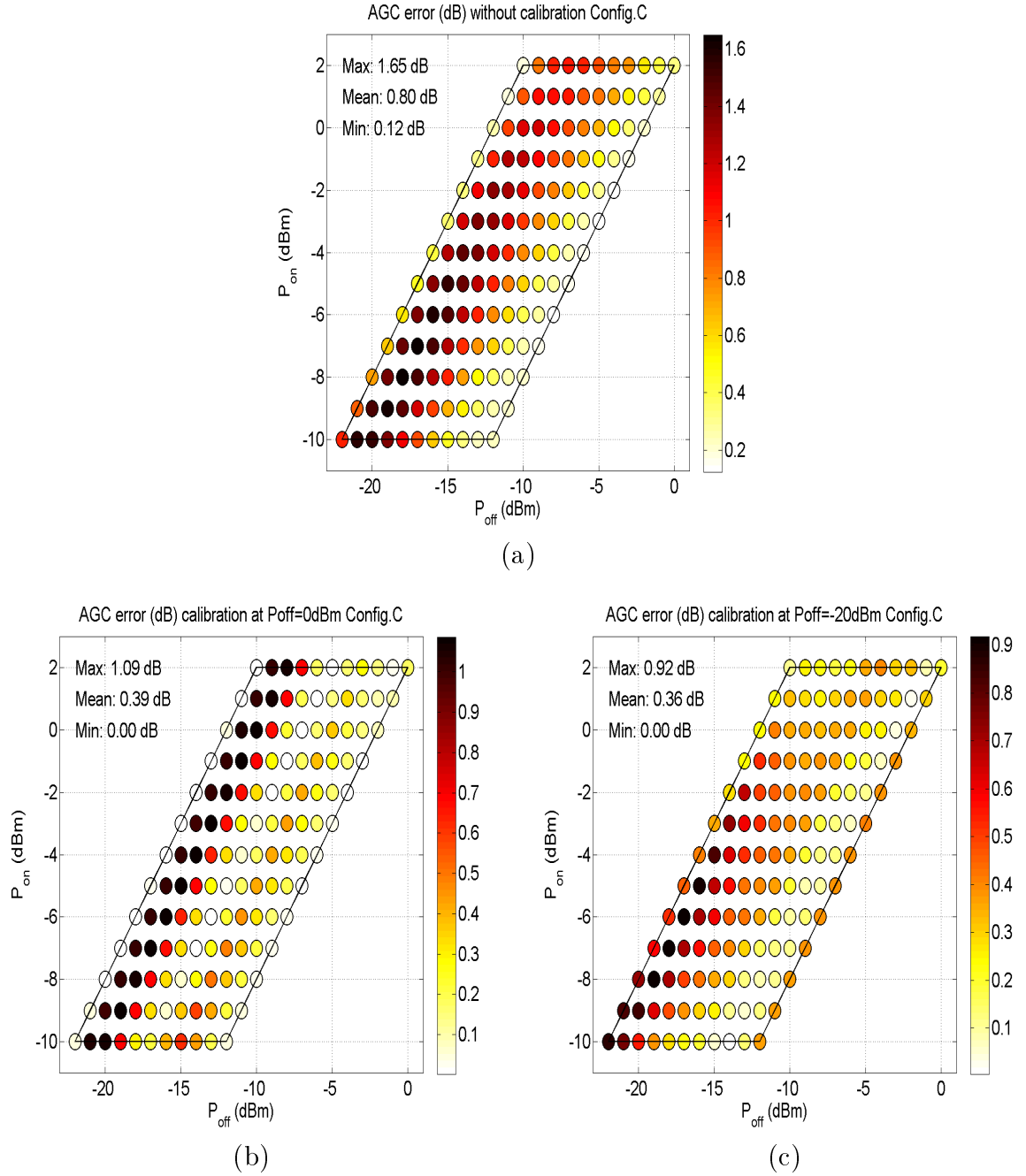

Figure C.3: Experimental results, configuration C: (a) before calibration; (b) calibration at $P_{off} = 0$ dBm; (c) calibration at $P_{off} = -20$ dBm.